Introduction to Sound Propagation Under Water

6

Christine Erbe, Alec Duncan, and Kathleen J. Vigness-Raposa

6.1 Introduction

It is imperative that bioacousticians who work in aquatic environments have a basic understanding of sound propagation under water. Whether the topic is the function of humpback whale song, echolocation in wild bottlenose dolphins, the masking of grey whale sounds by ship noise, the role of chorusing in fish spawning behavior, the effects of seismic surveying on benthic organisms, or the capability of an echosounder to track a school of fish, the way in which sound propagates through the ocean affects how we can use sound to study animals, how sound we produce impacts animals, and how animals use sound.

Aquatic fauna has evolved to use sound for environmental sensing, navigation, and communication. This is because water conducts sound very well (i.e., fast and far), while light propagates poorly under water. Visual sensing based on sun- or moonlight is limited to the upper few meters of water. And while water transports chemicals, chemoreception is most effective over short ranges, where chemical concentration is high. Furthermore, sound can be detected from all directions, providing omnidirectional alerting of activities happening in the environment.

Given that sound may propagate over very long ranges with little loss, a myriad of sounds is commonly heard at any one place. These sounds may be grouped by origin: abiotic, biotic, and anthropogenic. Natural, geophysical, abiotic sound sources include wind blowing over the ocean surface, rain falling onto the ocean surface, waves breaking on the beach, polar ice breaking under pressure and temperature influences, subsea volcanoes erupting, subsea earthquakes rumbling along the seafloor, etc. Biotic sound sources include singing whales, chorusing fishes, feeding urchins, and crackling crustaceans. Anthropogenic sources of sound include ships, boats, fish-finding echosounders, oil rigs, gas wells, subsea mines, dredgers, trenchers, pile drivers, naval sonar, seismic surveys, underwater explosions, etc.

As these sounds travel from their source through the environment, they may follow multiple propagation paths. Sounds may be reflected at the sea surface and seafloor. Some sound may travel through the seafloor and radiate back into the water some distance away. Sound is scattered by scatterers in the water (such as gas bubbles or fish swim bladders). Sound bends as the ocean is layered with pressure, temperature, and salinity changing as a function of depth, and with freshwater inputs. All of these phenomena depend on the frequency of sound. The spectrum of broadband sound changes, too, as acoustic energy at

C. Erbe (✉) · A. Duncan
Centre for Marine Science and Technology, Curtin University, Perth, WA, Australia
e-mail: c.erbe@curtin.edu.au; A.J.Duncan@curtin.edu.au

K. J. Vigness-Raposa
INSPIRE Environmental, Newport, RI, USA
e-mail: kathy@INSPIREenvironmental.com

C. Erbe, J. A. Thomas (eds.), *Exploring Animal Behavior Through Sound: Volume 1*,
https://doi.org/10.1007/978-3-030-97540-1_6

high frequencies is more readily scattered and absorbed than energy at low frequencies. The receiver of sound can thus infer information not just about the source of sound but also about the environment's complexity.

Understanding the physics of sound in water is an important step in studies of aquatic animal sound usage and perception, whether these are conspecific social sounds, predator sounds, prey sounds, navigational clues, environmental sounds, or anthropogenic sounds. It is also critical for the study of impacts of sound on aquatic fauna, and for using passive or active acoustic tools for monitoring aquatic fauna and mapping biodiversity. The goal of this chapter is to introduce the basic concepts of sound propagation under water.

6.2 The Sonar Equation

The sonar equation was developed by the US Navy to assess the performance of naval sonar systems. These sonar systems were designed to detect foreign submarines. The sonar emits an acoustic signal under water and listens to returning echoes. The time of arrival and acoustic features of the echo may determine not only from what target the signal reflected, but also the range and speed of the target. The term "sonar" stands for "SOund Navigation And Ranging."

There are numerous forms of the sonar equation. What they all have in common is that (1) they each represent an equation of energy conservation, meaning that the total acoustic energy on either side of the equation is the same; and (2) all of the terms in the equation are expressed in decibel (dB). The sonar equation with its original terms as defined in Urick (1983) allows an easy conceptual exploration of various scenarios encountered in bioacoustics. The definitions and notations of some of the terms are more mathematically specific in the recent underwater acoustics terminology standard (ISO 18405)[1].

6.2.1 Propagation Loss Form

As sound propagates through the ocean, it loses energy, termed propagation loss (PL[2]). A simple form of the sonar equation equates PL to the difference between the source level (SL) and the received level (RL) of sound (Urick 1983):

$$PL = SL - RL \text{ (propagation loss form)} \quad (6.1)$$

SL was defined by Urick as $10\log_{10}$ of the ratio of source intensity to reference intensity (see Chap. 4). *RL* was equal to $10\log_{10}$ of the ratio of received intensity to reference intensity. *PL* was computed as $10\log_{10}$ of the ratio of source intensity to received intensity.

For example, a whale-watching boat might have $SL = 160$ dB re 1 μPa^2 (in terms of mean-square pressure, which is proportional to intensity; see Chap. 4) and be located 100 m from a group of whales. If *PL* in this environment and over this range is 40 dB, then *RL* at the whales is 120 dB re 1 μPa^2 (Erbe 2002; Erbe et al. 2016a).

6.2.2 Signal-to-Noise Ratio Form

Another simple form of the sonar equation relates the RL of a signal to the background noise level ($NL = 10\log_{10}$ of the ratio of noise intensity to reference intensity):

$$SNR = RL - NL \text{ (signal-to-noise ratio form)} \quad (6.2)$$

SNR is the level of the signal-to-noise ratio, expressed in dB. For example, a call from a whale might have a received level $RL = 105$ dB re 1 μPa^2 at another whale; however, background noise at the time might be $NL = 115$ dB re 1 μPa^2 over the frequency band of the call. The *SNR* is −10 dB. Can the whale still hear the other one or does the noise mask the call?

Because the *SNR* is a negative number in this example, if one was just considering the relative levels of signal and noise, the animals would not

[1] International Organization for Standardization. (2017). *Underwater acoustics—Terminology (ISO 18405)*. Geneva, Switzerland.

[2] In this chapter, we italicize variables, but keep abbreviations as regular font; so PL is an abbreviation while *PL* is a variable.

be able to hear one another because the background noise level is much greater than the received signal level. However, animals (and sonar systems) can take advantage of spectral and temporal characteristics of a received sound, as is explained below. Therefore, in the example of beluga whales (*Delphinapterus leucas*) trying to communicate in icebreaker noise, the listening whale can indeed detect the call, because of the different spectral and temporal structures of call and noise (Erbe and Farmer 1998).

6.2.3 Forms to Assess Communication Masking

Acoustic communication under water remains an area of active research. In the conceptual model of Fig. 6.1, one animal (the sender) emits a signal, which travels through the habitat to the location of the receiver. Whether the receiver can hear the message depends on a number of factors that relate to the sender, the habitat, and the receiver. The level and spectral features of the signal will affect how far it propagates and how well it can be detected above the ambient noise in the environment. The locations of sender and receiver matter, not just the range between the two animals, but also at which depth each happens to be located. If the two animals are oriented towards each other, directional emission and reception capabilities will enhance signal detection. The environment changes the level and spectral characteristics of the signal by reflection, refraction, scattering, absorption, and spreading losses. The detection capabilities of the receiver can be quantified by the detection threshold, critical ratio, and other factors. Ambient noise in the environment can initiate anti-masking strategies at both the sender (e.g., increasing the source level) and receiver (e.g., orienting towards the signal). A sonar equation can be constructed to investigate each of these factors, as outlined in the following sections.

The basic sonar relation for the communication scenario in Fig. 6.1 is:

$$SL - PL - NL > DT \,(\text{basic signal detection form}),$$

where DT is the detection threshold of the receiver, expressed in dB. A sound is deemed detectable if the expression on the left side exceeds the detection threshold. In the absence of noise, DT equals the audiogram. Audiograms are measured by exposing an animal to pure-tone

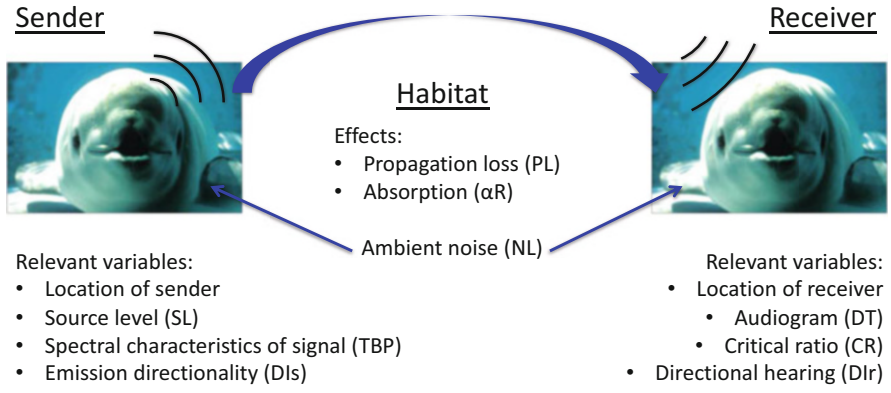

Fig. 6.1 Sketch of the factors related to acoustic communication in natural (not just aquatic) environments and their corresponding terms in the sonar equation: source level (SL), time-bandwidth product (TBP), sender directivity index (DIs), propagation loss (PL), absorption (absorption coefficient α multiplied by range R), noise level (NL), and receiver detection threshold (DT), critical ratio (CR), and directivity index (DIr). Modified from Erbe et al. (2016c); © Erbe et al. (2016); https://www.sciencedirect.com/science/article/pii/S0025326X15302125. Published under CC BY 4.0; https://creativecommons.org/licenses/by/4.0/

signals of varying levels. The RL that is just detectable defines the audiogram at that frequency (see Chap. 10 for a more thorough definition of audiogram):

$$RL = DT \text{ (audiogram form)}$$

The mammalian auditory system acts as a bank of overlapping bandpass filters and the listener focuses on the auditory band that receives the highest SNR (Moore 2013). Under the equal-power assumption (Fletcher 1940), a signal is detected if its power is greater than the noise power in any of the auditory bands. So, for any auditory band,

$$RL - NL > 0 \text{ (within an auditory band)} \quad (6.3)$$

Communication signals of many species, including birds and marine mammals (Erbe et al. 2017a), are commonly tonal, while noise is commonly broadband. In order to assess the risk of communication masking, the critical ratio (CR) is a useful quantity that has been measured in humans and animals. The CR is the level difference between the mean-square sound pressure level (SPL) of a tone and the mean-square sound pressure spectral density level of broadband noise when the tone is just audible (American National Standards Institute 2015). Conceptually, the CR quantifies the ability of the auditory system to focus on a narrowband (tonal) signal. It captures how many of the noise frequencies surrounding the tone frequency are effective at masking the tone, and the resulting band of frequencies has been termed the Fletcher critical band (American National Standards Institute 2015). A narrowband signal is thus detectable, if

$$RL - CR > NL_f \text{ (critical ratio form)} \quad (6.4)$$

RL is the tone level in dB re 1 μPa^2, NL_f is the noise mean-square pressure spectral density level in dB re 1 μPa^2/Hz, and CR is measured in dB re 1 Hz (see p. 29 in Erbe et al. 2016c).

In the above-mentioned study with beluga whales communicating amidst icebreaker noise, the beluga whale call consisted of a sequence of six tones with overtones from 800 to 1800 Hz, and the icebreaker's bubbler system noise was broadband and relatively unstructured in frequency and time (Fig. 6.2) (Erbe and Farmer 1998). The bandwidth of the call, expressed in dB, was $10\log_{10}(1800–800) = 30$ dB re 1 Hz (see Chap. 4 for definitions and formulae). Given

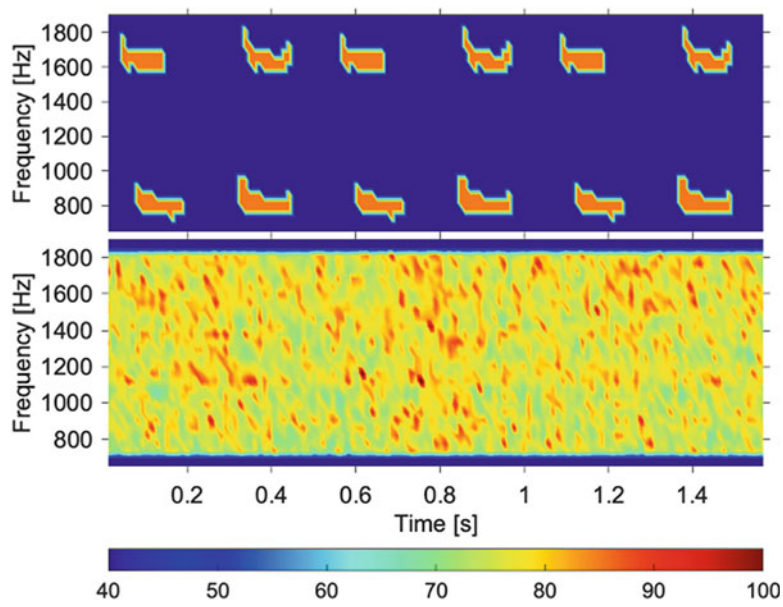

Fig. 6.2 Spectrograms of the lower two harmonics of a beluga whale call (top panel) and an icebreaker's bubbler system noise (bottom panel). Colorbar in dB re 1 μPa^2/Hz. The broadband levels are $RL = 105$ dB re 1 μPa^2 for the call and $NL = 115$ dB re 1 μPa^2 for the noise

$NL = 115$ dB re 1 μPa^2 over the bandwidth of the call, NL_f was equal to NL (115 dB re 1 μPa^2) minus the bandwidth (30 dB re 1 Hz): $NL_f = 85$ dB re 1 μPa^2/Hz. Beluga whales have a CR of approximately 15 dB re 1 Hz at 800 Hz, therefore, the call with $RL = 105$ dB re 1 μPa^2 was audible, because Eq. (6.4) was satisfied (Erbe 2008; Erbe and Farmer 1998): 105–15 > 85.

In studies on critical ratios and in the beluga whale experiments (Erbe and Farmer 1998; Erbe 2000), signal and noise were broadcast by the same loudspeaker and thus arrived at the listener from the same direction. If the caller and the noise are spatially separated, then there is an additional processing gain in the sonar equation: the receiver's directivity index *DIr*:

$$RL - CR + DIr - NL_f > 0$$
(critical ratio form with directivity index)

The *DIr* is defined as $10\log_{10}$ of the ratio of the intensity measured by an omnidirectional receiver to that of a directional receiver. Directivity indices increase with frequency and values up to 19 dB have been measured for communication sounds in marine mammals. The associated spatial release from masking should be considered in environmental impact assessments of underwater noise (Erbe 2015). Directivity indices are even greater at higher frequencies used by dolphins during echolocation (Fig. 6.3).

6.2.4 Form for Biomass Surveying

Surveys for animals ranging from zooplankton to fish and sharks may use an echosounder, fish finder, or sonar (e.g., Parsons et al. 2014; Kloser et al. 2013). In this scenario, the echosounder emits a signal, which travels to the fish, where some of it is reflected. How much of the signal is reflected is expressed by the target strength (TS), defined as $10\log_{10}$ of the ratio of echo intensity to incident intensity (Urick 1983). The reflected signal travels to the receiver, which has a specific *DT* and *DIr*. The receiver is typically co-located with the source, so that the signal travels the same path twice and thus experiences twice the PL. The fish is detected if the following sonar equation is satisfied:

$$SL - 2\,PL + TS - NL > DT - DIr$$
(two − way sonar surveying form)

Target strength will vary for each type of animal, as well as with the number of animals in the group and their orientation relative to the echosounder. Figure 6.4 shows reflected signals received on a REMUS autonomous underwater vehicle. Individual animals are observed in two aggregations, with two dolphins swimming within one of the aggregations. Researchers are using cameras on the same platforms to better understand the information contained in reflected

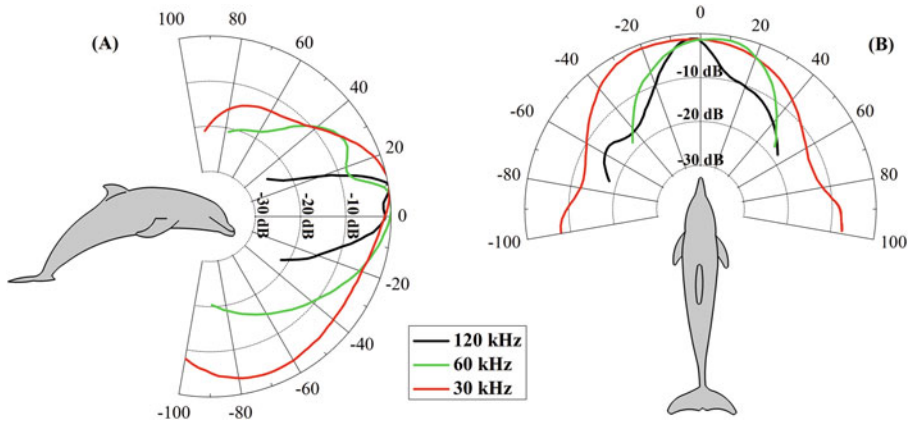

Fig. 6.3 Sketches of the receiving directivity pattern of a bottlenose dolphin (*Tursiops truncatus*) in the vertical (**a**) and horizontal (**b**) planes. Courtesy of Chong Wei after data in (Au and Moore 1984)

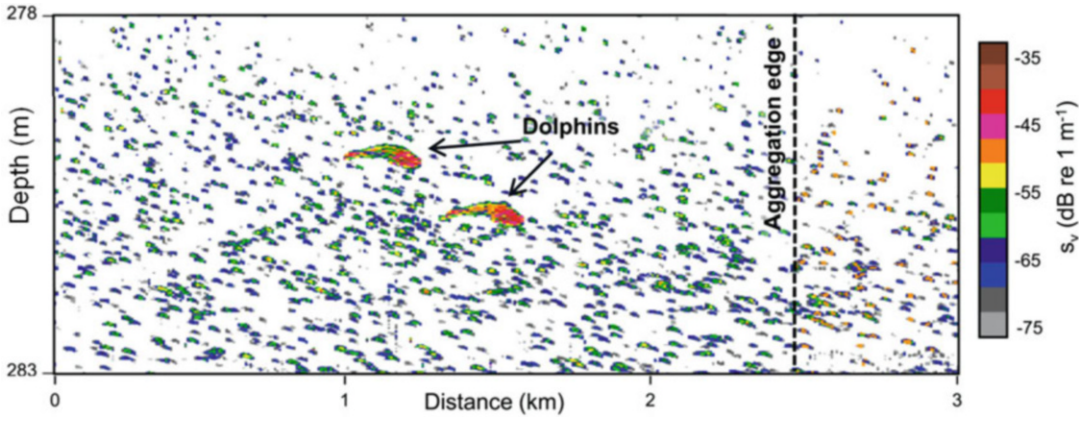

Fig. 6.4 Echosounder image of marine fauna in two aggregations, with two dolphins being in the aggregation on the left. Colors represent acoustic target strength and the shapes of the two dolphins can easily be recognized by their high reflectivity (Benoit-Bird et al. 2017). © Benoit-Bird et al. 2017; https://aslopubs.onlinelibrary.wiley.com/doi/full/10.1002/lno.10606. Published under CC BY 4.0; https://creativecommons.org/licenses/by/4.0/

signals and ultimately convert that information into species classifications and estimates of biomass (Benoit-Bird and Waluk 2020).

6.3 The Layered Ocean

The speed of sound in sea water increases with increasing temperature T [°C], salinity S (measured in practical salinity units [psu]) and hydrostatic pressure, which in the ocean is proportional to depth D [m]. The approximate change in the speed of sound c [m/s] with a change in each property is:

- Temperature changes by 1 °C → c changes by 4.0 m/s
- Salinity changes by 1 psu → c changes by 1.4 m/s
- Depth (pressure) changes by 1 km → c changes by 17 m/s

Maps of sea surface temperature and salinity for the northern hemisphere summer show considerable variation (Fig. 6.5). However, temperature and salinity vary much more rapidly with depth than they do in the horizontal plane, so the ocean can often be thought of as a stack of horizontal layers, with each layer having different properties. Vertical profiles of these quantities are therefore very useful for understanding how sound will propagate in different geographical regions.

6.3.1 Temperature and Salinity Profiles

In non-polar regions (red curves in Fig. 6.6), the main source of heat entering the ocean is solar. The sun heats the near-surface water, making it less dense and suppressing convection. A surface mixed layer with nearly constant temperature and salinity is formed by mechanical mixing due to surface waves and is typically 20–100 m thick. Below that, the temperature drops rapidly in a region known as the thermocline, before becoming almost constant at a temperature of about 2 °C in the deep isothermal layer that extends from a depth of about 1000 m to the ocean floor.

Seasonal changes in solar radiation together with the ocean's considerable thermal lag (due to its great heat capacity) can complicate this simple picture, but most of these changes only affect the top few hundred meters of the water column, changing the detailed structure of the mixed layer and the upper part of the thermocline.

In polar regions (blue curves in Fig. 6.6), the situation is quite different. There is a net loss of

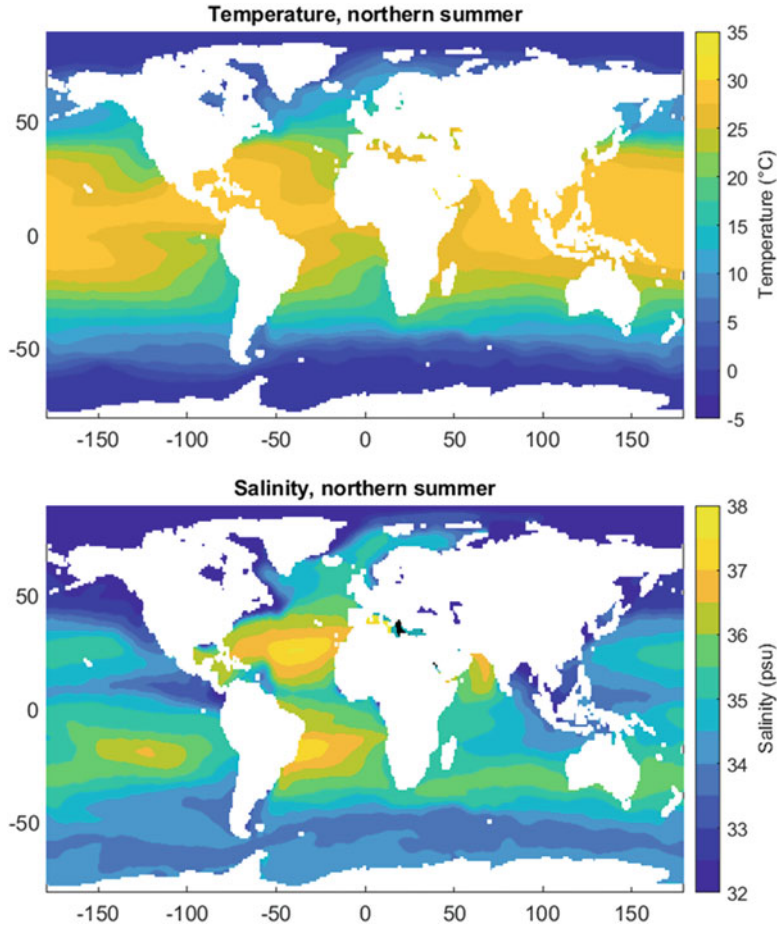

Fig. 6.5 Maps of sea surface temperature (top) and salinity (bottom) for the northern hemisphere summer, averaged over the period 2005 to 2017. Data were taken from the *World Ocean Atlas* (Locarnini et al. 2018; Zweng et al. 2018)

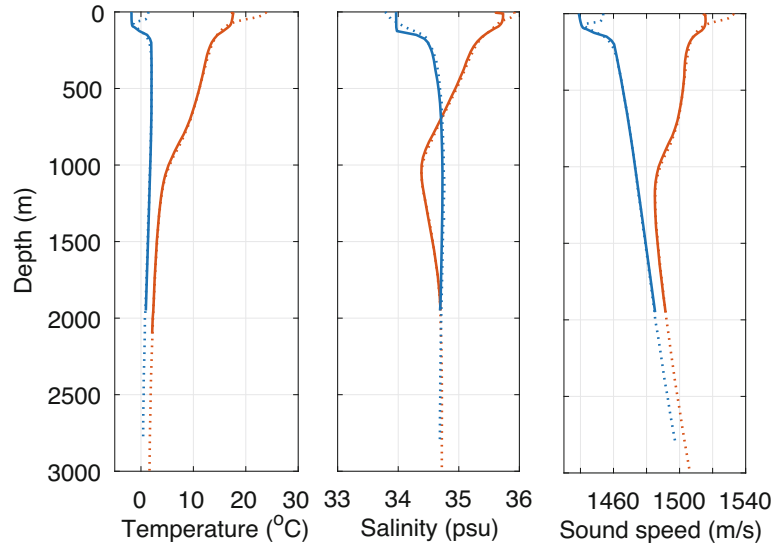

Fig. 6.6 Depth profiles of temperature, salinity, and sound speed from the open ocean based on the *World Ocean Atlas* (Locarnini et al. 2018; Zweng et al. 2018) seasonal decadal average data for the austral winter (solid) and austral summer (dotted). Red curves are for 30.5°S, 74.5°E and are representative of non-polar ocean profiles. Blue curves are for 60.5°S, 74.5°E and are representative of polar ocean profiles

heat from the sea surface, which results in a temperature profile in the upper part of the ocean that increases with increasing depth from a minimum of about −2 °C at or (in summer) slightly below the surface.

Salinity typically changes by only a small amount with depth, and in most parts of the ocean is between 34 and 36 psu. As a result, the sound speed is usually determined by temperature and depth, however, salinity can have an important effect on sound speed in situations where it changes abruptly. Examples include locations where there is a large freshwater outflow into the ocean from a river, or in estuaries where it is common to have a wedge of dense, saline water underlying a surface layer of freshwater. In polar regions, the salinity of near-surface water can vary considerably depending on whether sea ice is forming, a process that excludes salt and therefore increases salinity in the water below the ice. When sea ice melts, freshwater is released, reducing near-surface salinity.

6.3.2 Sound Speed Profiles

The following equation is one of a number of equations of varying complexity that can be found in the literature relating the speed of sound to temperature, salinity, and depth (Mackenzie 1981). It is valid for temperatures from −2 to 30 °C, salinities of 30 to 40 psu, and depths from 0 to 8000 m.

$$\begin{aligned} c = {} & 1448.96 + 4.591\,T - 5.304 \times 10^{-2}\,T^2 \\ & + 2.374 \times 10^{-4}\,T^3 + 1.340\,(S-35) \\ & + 1.630 \times 10^{-2}\,D + 1.675 \times 10^{-7}\,D^2 \\ & - 1.025 \times 10^{-2} T(S-35) - 7.139 \\ & \times 10^{-13}\,TD^3\ [\mathrm{m/s}] \end{aligned}$$

Sound speed profiles computed from the typical temperature and salinity profiles are also plotted in Fig. 6.6.

In non-polar waters, the sound speed may increase slightly with depth in the mixed layer due to its pressure dependence, however, diurnal heating and cooling effects can eliminate or enhance this effect. As explained later in this chapter, whether or not there is a distinct increase in sound speed with depth in the mixed layer determines whether there is a surface duct, which has a considerable impact on acoustic propagation from near-surface sound sources and to near-surface receivers.

Below the mixed layer, the rapid reduction in temperature with depth (i.e., in the thermocline) results in sound speed also reducing until, at a depth of about 1000 m, the temperature becomes nearly constant. In the deeper isothermal layer, the increasing pressure results in the sound speed starting to increase with depth. There is therefore a minimum in the sound speed in non-polar waters at a depth of approximately 1000 m, which, as will be seen later, is important for long-range sound propagation.

In polar waters, the temperature and pressure both increase with increasing depth, so the sound speed also increases, which results in a strong surface duct. However, in the Arctic Ocean, the existence of water masses with different properties entering from the Pacific and Atlantic oceans can lead to more complicated sound speed profiles.

Temperature and salinity profiles for the world's oceans can be found in the *World Ocean Atlas*[3] (Locarnini et al. 2018; Zweng et al. 2018). These are based on averages of a large amount of measured data and are very useful for calculating estimated sound speed profiles for particular locations for particular months or seasons of the year. The real ocean is, however, highly variable; particularly the upper thermocline and mixed layer, which can change on time scales of hours, and in some extreme cases, tens of minutes, so there is no substitute for in situ measurements of temperature and salinity profiles to support acoustic work.

[3] *World Ocean Atlas* https://www.nodc.noaa.gov/OC5/woa18/; accessed 30 September 2020.

6.4 Propagation Loss

The apparent simplicity of the propagation loss term (i.e., *PL*) in the various sonar equations hides a great deal of complexity. There are a few special situations in which *PL* can be calculated quite accurately using simple formulae, and a few more in which it might be possible to obtain a reasonable estimate using a more complicated equation, but for everything else, these simple approaches can lead to large errors, and it is necessary to resort to numerical modeling. To further complicate matters, there are a number of different types of numerical models used for propagation loss calculations, each with its own assumptions and limitations, and it is important to be familiar with these so that the most appropriate model can be used for a given task.

6.4.1 Geometric Spreading Loss

The most basic concept of propagation loss is that of geometric spreading, which accounts for the fact that the same sound power is spread over a larger surface area as the sound propagates further from the source. The intensity is the sound power per unit area (see Chap. 4), so the increase in surface area results in a reduction in intensity. The simplest case is when the source is small compared to the distances involved, the sound speed is constant, and the boundaries (i.e., sea surface, seabed, and anything else that might reflect sound) are sufficiently far away that reflected energy can be ignored. In this situation, the acoustic wavefront forms the surface of a sphere. As the wavefront propagates outward, the radius r of the sphere increases, the surface area of the sphere increases in proportion to r^2, and therefore the intensity decreases inversely proportional to r^2. This leads to the well-known spherical spreading equation for PL:

$$PL = 20\log_{10}(r/1\text{m}) \tag{6.5}$$

Equation (6.5) is also applicable to calculating geometric spreading loss for sound radiated by a directional source, such as an echosounder transducer, or a dolphin's biosonar, providing the range is sufficiently large (i.e., the receiver is in the acoustic far-field of the source; see Chap. 4), and the above assumptions are all met.

Another situation in which spreading loss can be calculated analytically is when the sound is constrained in one dimension by reflection and/or refraction, so it can only spread in the other two dimensions. In underwater acoustics, this most commonly happens when the sound is constrained in the vertical direction by the sea surface or seafloor, but can still spread in the horizontal plane. The result is that the acoustic wavefront forms the surface of a cylinder, the area of which is proportional to the range. The intensity is therefore inversely proportional to the range, and the PL is given by the cylindrical spreading equation:

$$PL = 10\log_{10}(r/1\text{m}) \tag{6.6}$$

Some situations in which cylindrical spreading can occur are discussed later in this chapter, but it should be noted that Eq. (6.6), strictly speaking, only applies at *all* ranges from the source in the highly unusual case that the source is a vertical line source that spans the entire depth interval into which the sound is constrained, and that no sound is lost into either the upper or lower layers.

For the much more common case of a small source, the sound will undergo spherical spreading at short ranges where the boundaries have no effect, followed by cylindrical spreading at long ranges where the fact that the source has a small vertical extent is of little consequence. In between, there will be a transition region in which neither formula is accurate. This situation can be approximated by assuming a sudden transition from spherical to cylindrical spreading at a "transition range" r_t. Equation (6.7) applies only to ranges $r \gg r_t$ and still makes the assumption that there are no losses at the boundaries.

$$\begin{aligned} PL &= 20\log_{10}\left(\frac{r_t}{1\text{m}}\right) + 10\log_{10}\left(\frac{r}{r_t}\right) \\ &= 10\log_{10}\left(\frac{r_t}{1\text{m}}\right) + 10\log_{10}\left(\frac{r}{1\text{m}}\right) \end{aligned} \tag{6.7}$$

In shallow-water situations, some authors recommend using a transition range equal to the

water depth; however, while useful for very rough *PL* estimates, this approach should be adopted with caution as the best choice will depend on the characteristics of the seabed. The only way to accurately determine r_t for a given situation is to carry out numerical propagation modeling, in which case you might as well use that to directly determine the propagation loss, removing the need for (Eq. 6.7) and its inherent inaccuracies.

6.4.2 Absorption Loss

When a sound wave propagates through water, it results in a periodic motion of the molecules present in the water, and the slight friction within and between them converts some of the sound energy into heat, reducing the intensity of the sound wave. This is called absorption loss and results in a propagation loss that is proportional to the range traveled:

$$PL = \alpha r_{\mathrm{km}} \tag{6.8}$$

where r_{km} is the range in kilometers and α is the absorption coefficient in dB/km. The propagation loss due to absorption must be added to the propagation loss due to geometrical spreading described in Sect. 6.4.1.

A commonly used formula for α is:

$$\begin{aligned}\alpha = {} & 0.106\frac{f_1 f^2}{f_1^2+f^2}e^{(pH-8)/0.56} \\ & + 0.52\left(1+\frac{T}{43}\right)\frac{S}{35}\frac{f_2 f^2}{f_2^2+f^2}e^{-z/6} \\ & + 4.9\times 10^{-4} f^2 e^{-(T/27+z/17)}\end{aligned} \tag{6.9}$$

with $f_1 = 0.78(S/35)^{1/2}\mathrm{e}^{T/26}$ and $f_2 = 42\mathrm{e}^{T/17}$; f [kHz], α[dB/km]

valid for $-6 < T < 35°\mathrm{C}$ ($S = 35$psu, pH = 8, $z = 0$)
$7.7 < \mathrm{pH} < 8.3$ ($T = 10°\mathrm{C}$, $S = 35$psu, $z = 0$)
$5 < S < 50$psu ($T = 10°\mathrm{C}$, pH = 8, $z = 0$)
$0 < z < 7$km ($T = 10°\mathrm{C}$, $S = 35$psu, pH = 8)

(François and Garrison 1982a, b; Ainslie and McColm 1998).

The absorption coefficient increases with frequency (Fig. 6.7). At low frequencies, it is dominated by molecular relaxation of two minor constituents of seawater: $B(OH)_3$ and $MgSO_4$, whereas above a few hundred kHz, it is primarily due to the water's viscosity.

In summary, Fig. 6.8 compares how propagation loss increases with range for spherical spreading (Eq. 6.5), cylindrical spreading (Eq. 6.6), and combined spherical/cylindrical spreading with a transition range of 100 m (Eq. 6.7). The effect of absorption (Eq. 6.8) in addition to spherical spreading is also shown for frequencies of 1, 10, and 100 kHz.

6.4.3 Additional Losses

6.4.3.1 The Air–Water Interface

Reflection and Transmission Coefficients

In animal bioacoustics as well as noise research, one typically deals with sounds in one medium (i.e., either air or water) and then sticks to this medium, only modeling propagation within this medium and only considering receivers in this medium. However, sound does cross into other media, and so a fish might be able to hear an airplane flying overhead, and a bird flying directly overhead might be able to hear a submarine's sonar (Fig. 6.9).

As sound hits an interface, the incident wave, in most situations, gives rise to a reflected wave and a transmitted wave[4] (also see Chap. 5, where reflection is explained based on Huygens' principle). The energy of the reflected wave remains within the medium of the incident sound, but the energy of the transmitted wave is lost from the medium of the incident sound and transmitted into the adjacent medium. The amplitudes of the reflected and transmitted (plane) waves are given

[4] Dan Russell's animations of waves being reflected from hard and soft boundaries, and being transmitted: https://www.acs.psu.edu/drussell/Demos/reflect/reflect.html; accessed 12 October 2020.

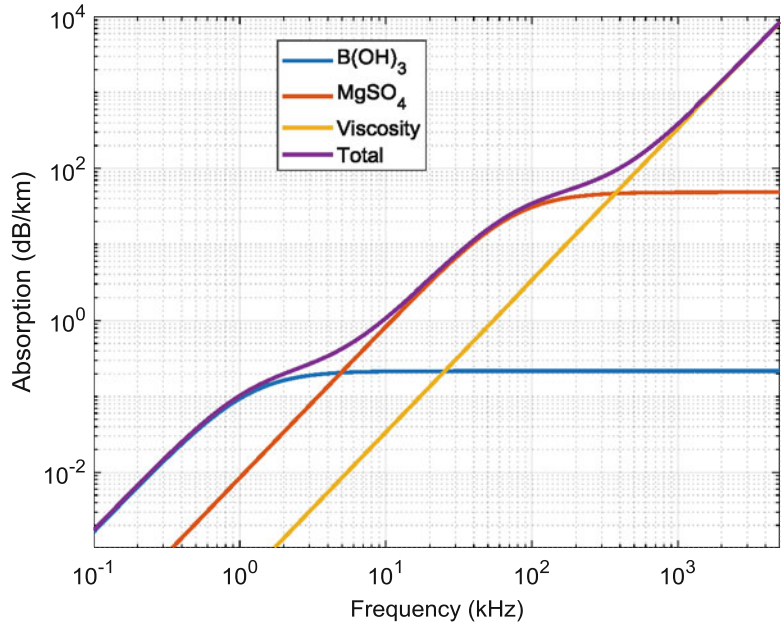

Fig. 6.7 Graph of absorption loss dominated by $B(OH)_3$ for $f < 5$ kHz, by $MgSO_4$ for 5 kHz $< f <$ 500 kHz, and by viscosity above. $T = 10$ °C, $S = 35$ psu, $z = 0$ m, pH $= 8$

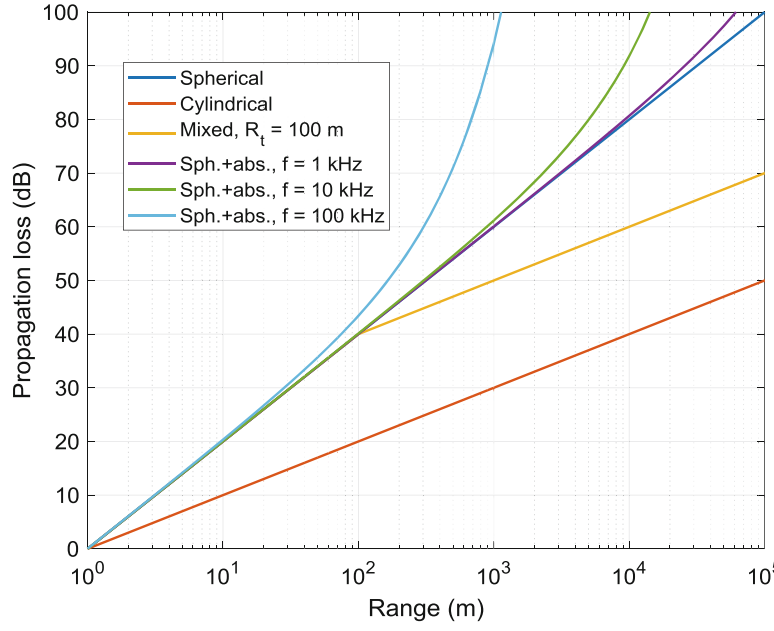

Fig. 6.8 Plot of propagation loss versus range assuming spherical spreading (Eq. 6.5), cylindrical spreading (Eq. 6.6), and mixed spherical/cylindrical spreading (Eq. 6.7) for a transition range of 100 m. Propagation loss is also shown for spherical spreading with the addition of absorption (Eq. 6.8) corresponding to frequencies of 1, 10, and 100 kHz. Note that in the literature, the y-axis is sometimes flipped

by the reflection and transmission coefficients $\mathcal{R}$ and $\mathcal{T}$ (Medwin and Clay 1998):

$$\mathcal{R} = \frac{Z_2 \sin\theta_1 - Z_1 \sin\theta_2}{Z_2 \sin\theta_1 + Z_1 \sin\theta_2} \tag{6.10}$$

$$\mathcal{T} = \frac{2Z_2 \sin\theta_1}{Z_2 \sin\theta_1 + Z_1 \sin\theta_2}$$

where θ_1 is the grazing angle of the incident wave, measured from the interface, and θ_2 is the grazing angle of the transmitted (refracted) wave, also measured from the interface. The angle of incidence is measured from the normal (i.e., perpendicular to the interface); the angle of incidence and the grazing angle of the incident wave always add to 90°. The acoustic impedance Z is the

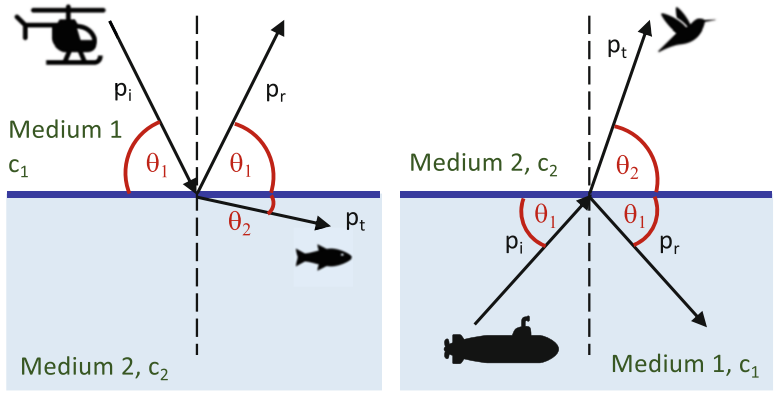

Fig. 6.9 Sketches of a sound source in the air (helicopter; left) and water (submarine; right), and the incident p_i, reflected p_r, and transmitted p_t rays (i.e., vectors pointing in the direction of travel, perpendicular to the wavefront), with corresponding grazing angles θ_1 and θ_2. In the left panel, medium 1 corresponds to air with sound speed c_1, and medium 2 corresponds to water with sound speed c_2. The situation is reversed in the right panel, where medium 1 is water, and medium 2 is air

product of density and sound speed: $Z = \rho c$. In air at 0 °C, $Z = 1.3$ kg/m^3 × 330 m/s = 429 kg/(m^{2}s). In freshwater at 5 °C, $Z = 1000$ kg/m^3 × 1427 m/s = 1,427,000 kg/(m^{2}s). In sea water at 20 °C and 1 m depth with 34 psu salinity, Z = 1035 kg/m^3 × 1520 m/s = 1,573,200 kg/(m^{2}s) (see Chap. 4). So, $Z_{air} << Z_{water}$, whether it is freshwater or saltwater.

Snell's law (Fig. 6.9, Eq. 6.11)[5] relates the angles of the incident and refracted waves (θ_1 and θ_2) at the interface. Rays bend towards the interface, if the speed of sound in medium 2 is greater than that in medium 1 ($c_2 > c_1$) and away from the interface, if $c_1 > c_2$. While Snell's law typically relates the sines of the angles measured from the normal, it may also be expressed in terms of the cosines of the grazing angles (Etter 2018):

$$\frac{\cos\theta_1}{\cos\theta_2} = \frac{c_1}{c_2} \tag{6.11}$$

For normal incidence, all of the angles in Eq. (6.10) are 90°, and so all of the sines are 1, hence

$$\mathcal{R} = \frac{Z_2 - Z_1}{Z_2 + Z_1} \text{ and } \mathcal{T} = \frac{2Z_2}{Z_2 + Z_1}$$

For a sound source in air, $Z_1 << Z_2 => \mathcal{R} \rightarrow 1$ and $\mathcal{T} \rightarrow 2$, at normal incidence. Almost all of the sound is reflected, but the pressure in the water increases by a factor 2. The air–water boundary, for sound arriving from air, is considered "hard." The value of $\mathcal{T}$ is the reason why even weak aerial sources (such as drones hovering over whales) can be detected in water, below the source, at several meters depth (Erbe et al. 2017b), and commercial airplanes can be recorded in coastal waters, lakes, and rivers even if flying at hundreds of meters in altitude (Erbe et al. 2018). Received levels under water from airplanes may exceed behavioral response thresholds for underwater sound sources (Kuehne et al. 2020). For non-normal incidence, with $c_2 > c_1$, there exists a critical angle, beyond which the transmitted wave disappears. This situation is called total internal reflection. The only sound in the water is an evanescent field that decays exponentially in amplitude below the sea surface. The evanescent field is only important if the depth of the receiver is smaller than the in-water acoustic wavelength.

For a sound wave meeting the water–air interface from below, $Z_1 >> Z_2$ therefore $\mathcal{R} \rightarrow -1$ and $\mathcal{T} \rightarrow 0$. Almost all sound is reflected, albeit at

[5] Dan Russell's animation of refraction and Snell's law: https://www.acs.psu.edu/drussell/Demos/refract/refract.html; accessed 12 October 2020.

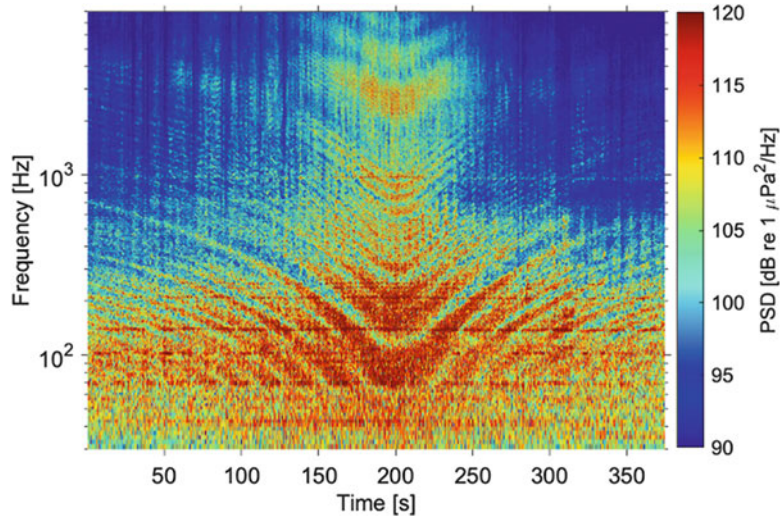

Fig. 6.10 Spectrogram of the recording of a ship passing by a moored recorder, showing the pattern of constructive and destructive interference called the Lloyd's mirror effect. The closest point of approach occurred at about 200 s. Modified from (Erbe et al. 2016c); © Erbe et al. 2016; https://www.sciencedirect.com/science/article/pii/S0025326X15302125. Published under CC BY 4.0; https://creativecommons.org/licenses/by/4.0/

negative amplitude, which means that the incident and reflected pressures cancel each other out. This is why the water–air interface is called a pressure-release boundary (or "soft" boundary) for sound incident from below. For non-normal incidence, $\mathcal{R}$ and $\mathcal{T}$ need to be computed with Eq. (6.10). Also, as a sound source is moved to shallower depth (i.e., closer to the sea surface), the proportion of transmitted sound increases. This is because of the evanescent (i.e., exponentially decaying) field, which is ignored by Eq. (6.10), but that might still have enough amplitude at the sea surface for shallow sources (Godin 2008).

Lloyd's Mirror

While not resulting in a loss of sound energy, the Lloyd's mirror effect is a result of reflection from the water–air interface from shallow sound sources. An omnidirectional source (i.e., one that emits sound in all directions) close to the sea surface (such as a ship's propeller) emits some of its sound in an upwards direction, and this sound reflects off the sea surface. At any receiver location, sound that traveled along the surface-reflected path overlaps with sound that traveled along the direct path from the source to the receiver. The reflected ray's amplitude is opposite in sign to the incident ray's amplitude ($\mathcal{R} = -1$); conceptually, this ray emerged from an image source (also called virtual source) with negative amplitude on the other side of the interface. The direct ray does not experience a flip in amplitude. Depending on the relative path lengths, the surface-reflected sound will add constructively to the sound that traveled along the direct path, or they will cancel each other out. This creates a pattern of constructive and destructive interference about the sound source, called the Lloyd's mirror effect. As a ship passes a moored recorder, the spectrogram shows the characteristic U-shaped interference pattern as successive peaks and troughs in amplitude at any one frequency over time (Fig. 6.10). Additional images of the Lloyd's mirror interference pattern can be found in (Parsons et al. 2020) for small electric ferries and in (Erbe et al. 2016b) for recreational swimmers and boogie boarders.

Scattering at the Sea Surface

If the sea surface is not flat, then some of the reflected energy is scattered away from the geometric reflection direction, reducing the amplitude of the geometrically reflected wave. This is called surface scattering loss, which increases as the roughness of the sea surface increases, the acoustic wavelength decreases (i.e., acoustic frequency increases), and the grazing angle between the direction of the incident wave and the plane of the sea surface increases. This relationship is quantified by the Rayleigh roughness parameter (Jensen et al. 2011):

$$\gamma = 4\pi \frac{h}{\lambda} \sin\theta \tag{6.12}$$

where h is the root-mean-square (rms) roughness of the surface (i.e., approximately ¼ of the significant wave height), λ is the acoustic wavelength, and θ is the grazing angle. The larger the value of γ is, the larger is the apparent roughness of the surface. The corresponding effective pressure reflection coefficient of the sea surface is then given by:

$$\mathcal{R}' = -e^{-0.5\gamma^2} \tag{6.13}$$

which corresponds to an additional propagation loss of $20 \log_{10}|\mathcal{R}'| = 4.34\gamma^2$ dB each time the sound reflects off the surface (Fig. 6.11). Note, however, that these formulae are only valid for surfaces that are not too rough, which, in this case, means $\gamma < 2$, corresponding to a scattering loss < 17 dB per bounce.

Strictly speaking, the effective pressure reflection coefficient (Eq. 6.13, Fig. 6.11) applies to the coherent component of the acoustic field, which can be thought of as the component that does not change as the rough sea surface moves. There will also be a scattered component that does change, and in some situations, this is an important contributor to the received signal. This component is ignored by Eq. (6.13), which can therefore be considered to provide an upper limit on the propagation loss per bounce.

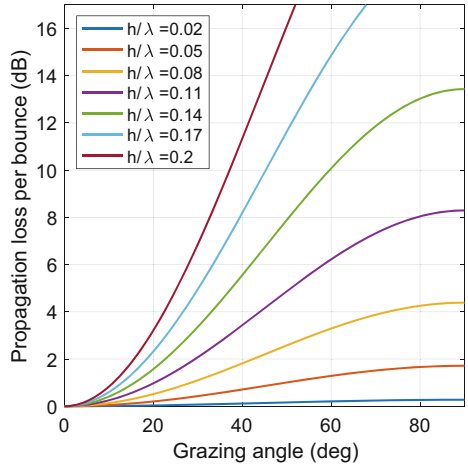

Fig. 6.11 Graphs of additional propagation loss per bounce as a function of grazing angle for reflection from rough surfaces with various ratios of rms roughness to acoustic wavelength

6.4.3.2 The Seafloor Interface

The interaction of sound with the seafloor is more complicated. The acoustic properties of the seabed are often similar to those of the water, so a significant amount of sound can penetrate the seabed. The lower the frequency is, the deeper the sound can penetrate. At frequencies below a few kHz, it is common for a significant amount of acoustic energy to be reflected back into the water column from geological layering within the seabed. Seismic survey companies searching for oil and gas reserves are taking advantage of this.

Some of this complexity is illustrated in Fig. 6.12, which plots the pressure reflection coefficient as a function of grazing angle for four different seabed types: silt, sand, limestone, and basalt. Silt and sand layers are unconsolidated, which means that shear waves have a low speed and attenuate rapidly. (Shear waves are waves in which the particles oscillate at right angles to the direction of sound propagation; see Chap. 4.) Acoustically, they can often be well approximated by a fluid (which does not support shear waves at all) with an increased attenuation to account for the shear wave losses.

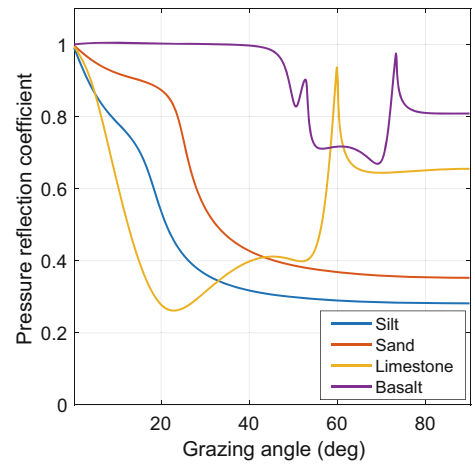

Fig. 6.12 Curves of pressure reflection coefficient versus grazing angle for four different seabed types, calculated with parameters from Jensen et al. (2011)

Unconsolidated sediments become more reflective as the sediment grain size increases from silt to sand. Limestone and basalt are consolidated rocks, which allow both compressional waves and shear waves to propagate, and are thus referred to as solid elastic seabeds. Basalt is a hard rock and highly reflective at all grazing angles. The reflection coefficient of limestone, however, is perhaps surprising. While it is also a rock, it has the lowest reflectivity of the four seabeds at small grazing angles. This is because the shear wave speed in limestone is very similar to the sound speed in water, which allows energy to pass easily from sound waves in the water to shear waves in the seabed.

Curves of reflection coefficients versus grazing angle are even more complicated for layered seabeds due to interference between waves reflecting from different layers, and in this case, the reflectivity becomes frequency dependent. Despite the complexity, there are computer programs available, based on techniques described in Jensen et al. (2011), that can numerically calculate the reflection coefficient curve for any arbitrarily layered seabed. A good example is *BOUNCE*, which is part of the *Acoustics Toolbox*.[6] A much bigger problem is the common lack of information on the geoacoustic properties of the seabed, to be able to provide these programs with accurate input data.

Seafloor roughness can further reduce the apparent acoustic reflectivity, although if the rms roughness is known, this can be dealt with (at least approximately) by using Eq. (6.12) to calculate the associated Rayleigh roughness parameter γ as a function of grazing angle. The effective seabed reflection coefficient is then:

$$\mathcal{R}' = \mathcal{R} e^{-0.5\gamma^2} \tag{6.14}$$

where $\mathcal{R}$ is the pressure reflection coefficient for the flat seafloor (Eq. 6.10). All terms in this equation depend on grazing angle. The propagation loss per bounce is given by $20 \log_{10} |\mathcal{R}'|$.

6.4.3.3 Scattering Within the Water Column

Sound can be scattered within the water column by anything that causes sharp changes in sound speed, density, or both (i.e., acoustic impedance, which is the product of sound speed and density; see Chap. 4). This includes gas bubbles, biological organisms (in particular those with gas-filled organs like lungs or swim bladders), and suspended sediment particles. Water column scattering is utilized in active sonar systems, which rely on the backscattered signal to detect and/or characterize objects within the water column. However, clouds of air bubbles formed by breaking waves can cause an appreciable increase in propagation loss in some circumstances.

Air bubbles are essentially small, resonant cavities within the water column, which can both scatter and absorb sound and, when found in large numbers, can change the effective density, and hence sound speed, of the water. When a wave breaks, it entrains a large amount of air down to depths of several meters, forming a cloud of bubbles of a range of sizes. The large bubbles rise to the surface quite quickly, but the smaller bubbles can remain at depth for many minutes. This can increase the propagation loss for sound traveling close to the surface (Ainslie 2005; Hall 1989).

6.4.4 Numerical Propagation Models

6.4.4.1 The Wave Equation and Solution Approaches

The ocean is a complicated environment for sound propagation, and the simple approaches to estimating propagation loss described above are very limited in their applicability. As a result, a great deal of effort has gone into developing numerical propagation models that can calculate acoustic propagation loss for realistic situations. What follows is a brief introduction to the topic. The interested reader is referred to Etter (2018)

[6] *Acoustics Toolbox:* https://oalib-acoustics.org/models-and-software/acoustics-toolbox/; accessed 30 September 2020.

and Jensen et al. (2011) for a more comprehensive treatise.

Fundamentally, all numerical propagation models solve the acoustic wave equation, which is a differential equation that relates the way the pressure changes over time to how it changes spatially as a wave propagates:

$$\nabla^2 \Phi = \frac{1}{c^2} \frac{\partial^2 \Phi}{\partial t^2} \tag{6.15}$$

where ∇^2 is the Laplace operator, ∂ indicates the partial derivative, c is the speed of sound, t represents time, and Φ is the solution to the wave equation.

The wave equation itself is well understood and straightforward to solve in simple cases; however, there are two issues that make it difficult to solve numerically for typical underwater acoustics problems:

1. Solutions are usually desired over domains that are orders of magnitude larger than the acoustic wavelength. Direct solution methods, such as finite differences or finite elements, require meshing the solution domain at a resolution of a small fraction of a wavelength, so the size of the required domain makes these approaches impractical for most propagation problems, even with modern computing hardware.
2. The boundaries of the domain, particularly the seabed, are complicated, but very important to model accurately as they have a strong influence on sound propagation.

Getting around these difficulties requires making approximations that lead to equations that are practical to solve for the problems of interest, with different approximations leading to different methods suitable for different situations.

In general, the solution of the acoustic wave equation is a function of three spatial dimensions and time. In Cartesian coordinates, the acoustic pressure can be written as: $p(x, y, z, t)$. In most cases, we are interested in the field generated by a small source, which can be approximated as a single point in space. It is more convenient to work in cylindrical coordinates centered on the source location, $p(r, z, \phi, t)$, where r is the horizontal distance from the source to the receiver, z is the receiver depth below the sea surface, and ϕ is the horizontal plane azimuth angle of the receiver relative to some direction reference.

Many modeling approaches start by assuming that the solution has a harmonic time dependence so that $p(r, z, \phi, t) = p_\omega(r, z, \phi)e^{-i\omega t}$ where $\omega = 2\pi f$ is the angular frequency and $i = \sqrt{-1}$. Substituting this solution form into the wave equation (Eq. 6.15) leads to another differential equation called the Helmholtz equation, which can be solved at a specified ω to give $p_\omega(r, z, \phi)$. The computational advantage of this is that the Helmholtz equation can be solved independently for each required frequency, converting a coupled four-dimensional (4D) problem into a number of independent 3D problems. Models that use this approach are known as frequency domain models, whereas models that directly solve the wave equation are known as time domain models. If required, the time domain solution can be reconstructed from multiple frequency domain solutions using Fourier synthesis (see Jensen et al. 2011, Chap. 8, for details).

The azimuth angle dependence can be dealt with by two different approaches. Modeling in 3D retains the full azimuth dependence of the environment, whereas $N \times$ 2D modeling assumes that changes in the environment due to small changes in ϕ have negligible effect on sound propagation, so that modeling can be carried out independently along each azimuth of interest. The majority of numerical models use the $N \times$ 2D approach, because there is again a substantial computational saving, this time by reducing a coupled 3D problem, solving for $p_\omega(r, z, \phi)$, to a number of independent 2D problems, each solving for $p_{\omega, \phi}(r, z)$ using only environmental information for the corresponding azimuth.

The inherent assumption of the $N \times$ 2D method provides a good approximation to the sound field in many propagation modeling situations where horizontal sound speed gradients are much smaller than vertical sound speed gradients, the seabed slopes are small, and the ranges are not large enough for the remaining out-of-plane effects to have an appreciable effect

on the sound field. However, there are cases where full 3D modeling may be required; for example, around steep-sided submarine canyons, in the presence of nonlinear internal waves that can produce strong horizontal sound speed gradients, or for very-long-range propagation across ocean basins.

Some propagation models further simplify their calculations by assuming that the environment (but not the sound field) is independent of range, which means that the sound speed profile is a function of depth only, and the water depth and seabed properties are the same at all ranges (i.e., the seafloor is flat). These are called range-independent (RI) propagation models, whereas propagation models that allow the sound speed profile and/or the water depth and/or the seabed properties to vary with range are known as range-dependent (RD) models.

Acoustic propagation models are usually characterized by the numerical approach adopted, and the following sections described some of the most common. Guidance on which propagation model to use in various scenarios follows this section.

6.4.4.2 Ray and Beam Tracing

A ray is a vector, normal to the wavefront, and shows the direction of sound propagation. Ray models trace rays by repeatedly applying Snell's law (Eq. 6.11). For layered media (such as layers of ocean water with differing properties), Snell's law relates the angles of incidence θ_1 and refraction θ_2 at every layer boundary. Rays bend towards the horizontal, if $c_2 > c_1$, and away from the horizontal if $c_1 > c_2$.

There are several approaches to calculating the amplitude of the acoustic field. The simplest, known as conventional ray tracing, is to use the distance between initially adjacent rays to determine the area over which the sound power has spread and calculate the intensity as the power per unit area. Unfortunately, this method results in unphysical predictions of infinite sound amplitude at locations called caustics, where initially adjacent rays cross and therefore have zero separation. It also predicts sharp transitions to zero sound intensity in shadow zones, which are regions where rays do not enter, whereas in reality, the transition will be smoother. Both of these problems are a result of a high-frequency approximation inherent in ray theory, which cannot deal with diffraction (i.e., the phenomenon of waves bending around obstacles or spreading out after passing through a narrow gap; see Chap. 5 on sound propagation examples in the terrestrial world).

An alternative approach to calculating the amplitude of the acoustic field is to treat each ray as the center of a beam with a specified (usually Gaussian) amplitude profile. The field at a particular location is then obtained by summing the contributions from all the beams that overlap at that location. The main challenge with this approach is determining how the amplitude and width of the beam should change along the ray, but algorithms have been developed to do this (see Jensen et al. 2011, Sect. 3.5, for details). One of the best-known propagation codes of this type is *Bellhop* (Porter and Bucker 1987), a fully range-dependent, Gaussian beam tracing program suitable for $N \times 2$D modeling that is available as part of the *Acoustics Toolbox*. The toolbox also includes a fully 3D variant called *Bellhop3D*.

Although Gaussian beam tracing is an improvement to conventional ray tracing and reduces the effects of the high-frequency assumption inherent in ray theory, it does not completely eliminate them. Its treatment of shadow zones and caustics produces realistic, but not necessarily accurate results and, importantly, it does not predict waveguide cutoff effects.

In underwater acoustics, the term waveguide or duct is used to describe any situation in which sound is constrained to a particular span of depths by reflection, refraction, or some combination of the two. Common examples include (Fig. 6.13):

1. A shallow-water duct in which sound is constrained by reflection from both the sea surface and the seabed.
2. A surface duct, in which the sound speed near the sea surface increases with increasing depth. This results in sound that is initially heading downward being refracted upwards towards the sea surface, where it is reflected back downward again, and so on. It is therefore constrained by reflection at the top and by

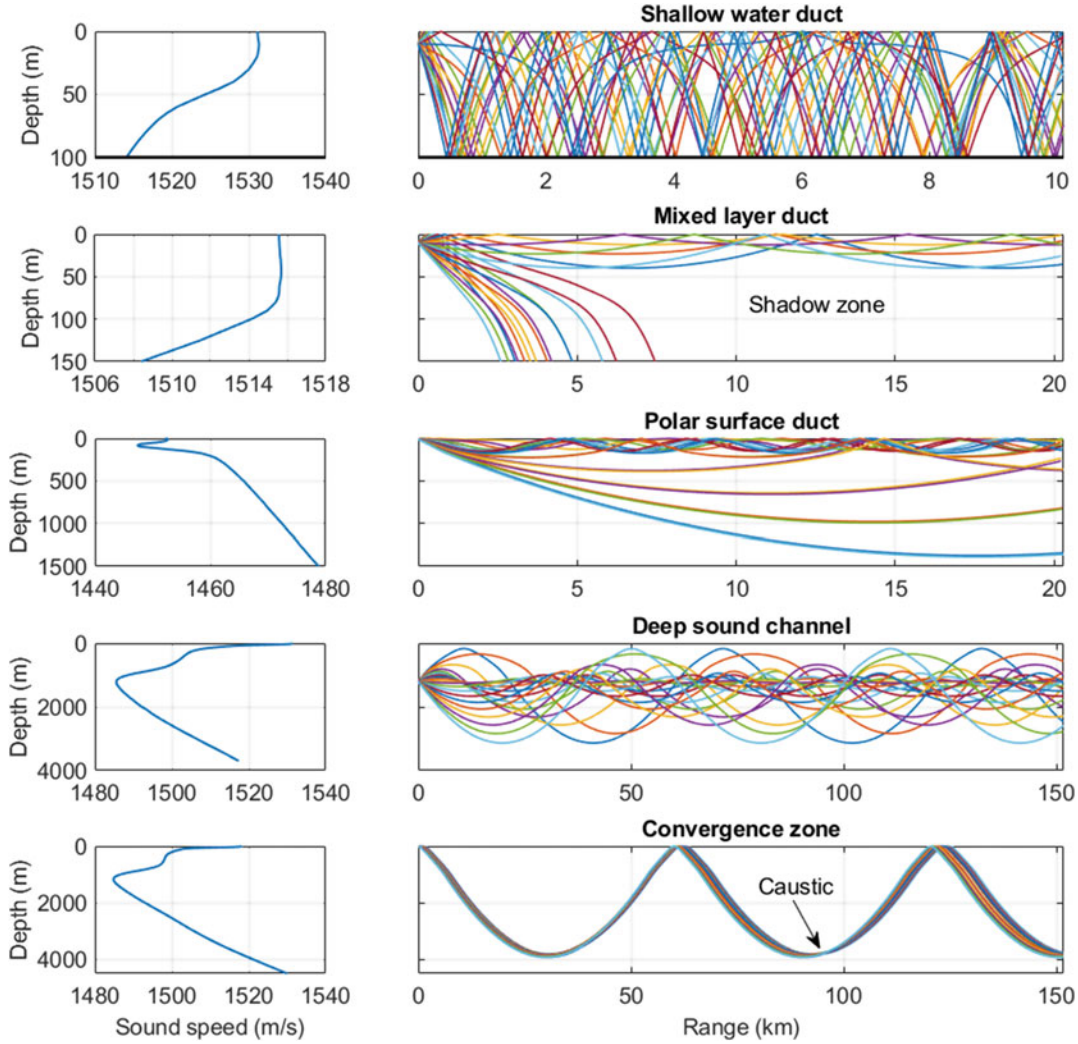

Fig. 6.13 Sound speed profiles (left) and ray trace plots computed using *Bellhop* (Porter and Bucker 1987, right) illustrating the common underwater acoustic ducts described in the text. The source depth was 10 m for all except the deep sound channel example, which had a source depth of 1200 m

refraction at the bottom. Weak surface ducts are often found in the mixed layer due to sound speed increasing with increasing pressure, and strong surface ducts are ubiquitous in polar oceans because both pressure and temperature increase with increasing depth. Sea ice can, however, reduce the acoustic reflectivity of the sea surface and therefore increase the attenuation of sound traveling in the duct.

3. The Deep Sound Channel (DSC), also known as the sound fixing and ranging (SOFAR) channel, in which sound is refracted towards the minimum in the sound speed (i.e., towards the waveguide axis). The waveguide axis occurs at a depth of about 1000 m in much of the world's ocean. The sound is constrained by refraction both above and below the axis of the waveguide. However, these are not sharp boundaries, and the steeper the angle of propagation is, the larger are the excursions of the ray paths away from the axis.
4. Convergence zone propagation in which sound is constrained by reflection from the sea surface and refraction from the increase

of sound speed with increasing depth that occurs below the axis of the DSC.

In all cases, the waveguide will only trap rays leaving the source within a certain span of angles from the horizontal. In the case of the shallow water waveguide, this is because the seabed reflectivity reduces as the grazing angle increases (Fig. 6.12), so more energy is lost on each bottom bounce at steeper angles. In the other waveguide cases, it is because the refraction is not strong enough to turn the ray around before it either reaches a depth where the sound speed gradient is refracting it away from the waveguide (surface duct) or it hits the seabed (DSC and convergence zone).

According to ray theory, rays can be launched at any angle, irrespective of the frequency, and so it should always be possible to find rays that will be trapped in the waveguide, provided the source is at a suitable depth. However, this is not actually the case at low frequencies, where the acoustic wavelength becomes an appreciable fraction of the thickness of the waveguide. It turns out that if the frequency is sufficiently low, no energy will be trapped in the waveguide, and the waveguide is said to be cut off. Understanding why this is the case requires an understanding of normal modes, which is the topic of the next section.

6.4.4.3 Normal Modes

Most people find the concept of normal modes to be less intuitive than that of rays, but it is very useful for understanding low-frequency sound propagation in the ocean and forms the basis for a class of acoustic propagation models called normal-mode models.

Normal modes are best understood by first considering an ideal shallow-water waveguide with a constant depth (i.e., flat seafloor), constant sound speed, and perfectly reflecting seafloor. Solving the Helmholtz equation for this situation requires that two so-called boundary conditions be met: one at the sea surface and one at the seafloor. The sea surface is a soft boundary as far as underwater sound is concerned, so the boundary condition here is that the acoustic pressure due to the incident and reflected waves sums to zero, which requires that an incident sound wave is inverted on reflection. Conversely, the seafloor is a hard boundary, which requires that the incident and reflected waves sum to a maximum pressure; so the amplitudes of the incident and reflected waves must have the same sign.

Both of these boundary conditions have to be satisfied simultaneously. The water depth is fixed, and normal modes consider one frequency at a time, so the wavelength is fixed. The only variable that can change to satisfy the requirements is the angle from the horizontal at which the wave propagates. There are certain, discrete propagation angles that allow the surface and seafloor boundary conditions to be met simultaneously, corresponding to the normal modes. Each normal mode consists of a pair of plane waves, one propagating upward and the other downward, at the same angle to the horizontal (Fig. 6.14). The mode that corresponds to the pair of waves propagating closest to the horizontal is called the lowest-order mode (mode 1), and the mode order increases as the propagation angle gets steeper. Note that the waves can never propagate exactly horizontally, because that does not meet the boundary conditions.

A receiver in the water column will receive the sum of the pressures from the upward and downward traveling waves. The amplitude of that combined signal can be plotted as a function of depth and range for each mode, yielding a series of mode shape curves (Fig. 6.15). Note that there is always a null in pressure (i.e., a node) at the sea surface and a maximum in pressure magnitude (i.e., $+1$ or -1; an antinode) at the hard seafloor.

The mode shapes are reminiscent of standing waves on a guitar string, which are also normal modes. However, on a guitar string, different modes correspond to different frequencies of vibration, whereas in a waveguide, different modes correspond to sound of the same frequency propagating at different angles to the horizontal.

For any waveguide thickness, the propagation angles for a particular mode increase as frequency is reduced. The ideal waveguide considered so far has no limit to how steep the propagation angles can be, but that is not the case for real ocean

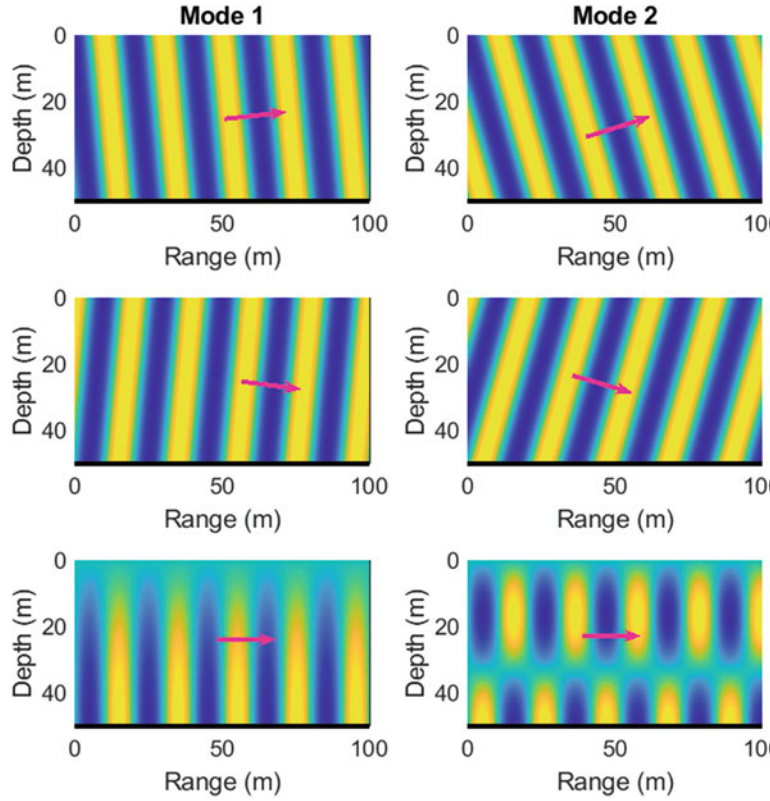

Fig. 6.14 Depth-range plots showing how the normal modes of an ideal shallow-water waveguide (lower panel) result from a pair of upward (upper panel) and downward (middle panel) propagating plane waves. Left-hand panels are for mode 1, right-hand panels are for mode 2. Arrows show the direction of propagation. The water depth is 50 m and the acoustic wavelength is 20 m

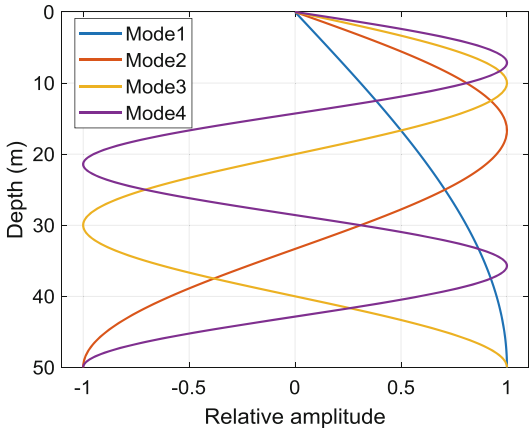

Fig. 6.15 Mode shapes for the first four normal modes of a 50-m deep ideal shallow-water waveguide with a rigid seabed

waveguides which, as discussed in the previous section, all have limits on the angular range of the energy they can trap. The highest-order mode corresponds to the steepest propagation angle, so as frequency is reduced, it will become too steep to be constrained by the waveguide and will no longer be able to propagate. As frequency is reduced further, the same will happen to the next-highest-order mode, and so on until the lowest-order mode is unable to propagate, at which point the waveguide is said to be cut off.

In real ocean waveguides, the sound speed varies with depth, which causes the propagation angle of each mode to also be a function of depth. This changes the mode shapes, but you can still consider a mode to consist of a pair of upward and downward going waves, propagating at the same angle to the horizontal at any given depth.

The starting point for the mathematical derivation of normal-mode models is the depth-separated Helmholtz equation, which is valid for range-independent problems and is obtained by assuming that the acoustic field can be represented by the product of a function of depth and a function of range:

$$p_{\omega,\phi}(r,z) = F(z)G(r).$$

Substituting this into the Helmholtz equation results in a one-dimensional differential equation for $F(z)$ in terms of a separation constant k_r. The solution of this differential equation has poles (infinities) at certain values of k_r, which correspond to the normal modes. Normal-mode codes search for these values of k_r, calculate the corresponding mode shapes, and then compute $p_{\omega,\phi}(r, z)$ by a mathematical technique called the "method of residues," which involves summing the contributions of all the poles, which in this case, corresponds to summing the contributions of the individual modes. It turns out that k_r has a geometric interpretation. It is called the horizontal wavenumber and is related to the modal propagation angle θ (relative to the horizontal) by $k_r = \omega \cos(\theta)/c$.

Normal-mode codes are computationally very fast for range-independent problems, because the modes only have to be found once, after which the field can be calculated at any desired range with very little additional computational effort.

Dealing with range-dependent problems involves approximating the environment as a series of range-independent sections, calculating the modes for each of these sections, and then calculating how the energy present in the modes in one section transmits across the boundary to the modes in the next section. There are two approaches:

1. The adiabatic mode method assumes that all the energy in mode 1 stays in mode 1, all the energy in mode 2 stays in mode 2, etc. This is relatively simple to implement and fast to compute, but is only accurate for environments that change relatively slowly with range.
2. The coupled-mode method allows energy to transition between modes, and so can deal with environments that change more rapidly. But this method is much more computationally demanding.

A good example of a normal-mode model is *KRAKEN* (Porter and Reiss 1984), which can be used for both range-independent and range-dependent modeling (both adiabatic and coupled) and is part of the *Acoustics Toolbox* (Footnote 5).

One limitation of normal-mode models such as *KRAKEN* is that they only include the component of the acoustic field that is fully trapped in the waveguide, so they tend to be inaccurate at short ranges where the component of the field that is losing energy out of the waveguide can be significant. This problem can be addressed by including so-called leaky modes in the solution. However, reliably finding leaky modes turns out to be a very challenging numerical task. The most successful normal-mode model to-date in this respect is *ORCA* (Westwood et al. 1996), which is accurate at short range and can also deal with seabeds that support shear waves. *ORCA* was written as a range-independent model, but there have been several attempts to adapt it to range-dependent problems using the adiabatic mode method (Hall 2004; Koessler 2016).

6.4.4.4 Wavenumber Integration

The mathematical derivation of the wavenumber integration method also starts with the depth-separated Helmholtz equation, but in this case, $F(z)$ is calculated by direct numerical solution of the one-dimensional differential equation over a range of k_r values, giving the so-called wavenumber spectrum. The acoustic field $p_{\omega,\phi}(r, z)$ is then obtained by an integral transform of the wavenumber spectrum that involves a Hankel function. A numerical approximation to the Hankel function that is valid except at ranges smaller than the acoustic wavelength can be used to convert this integral transform into a Fourier transform, which can then be evaluated using the very efficient Fast Fourier Transform algorithm.

Wavenumber integration codes that use this method of evaluating the integral transform are known as fast-field programs. Common examples are *SAFARI*, *OASES*, and *SCOOTER* (Porter 1990; Schmidt and Glattetre 1985). *OASES* is a development of *SAFARI* and has largely superseded it, whereas *SCOOTER*, which is part of the *Acoustics Toolbox* (Footnote 5), is a separate, but largely equivalent, development. These programs are very accurate for acoustic propagation calculations at ranges close enough to the source that the environment can be considered range-independent, and can deal with arbitrarily complicated, layered seabeds. For

most applications, the short-range limitation introduced by the Hankel function approximation is of little consequence, but, if necessary, it can be removed (at additional computational cost) by directly evaluating the integral transform.

It has proved difficult to extend the wavenumber integration method to range-dependent problems in a way that results in an efficient propagation model, although the full (paid) version of *OASES*[7] does have this capability. The theoretical background of this model is described in Goh and Schmidt (1996).

6.4.4.5 Parabolic Equation

Inserting a solution of the form $p_{\omega,\phi}(r,z) = f(r,z)H_0^{(1)}(k_0 r)$ into the Helmholtz equation yields parabolic-equation (PE) models. Here, $H_0^{(1)}$ represents an outgoing cylindrical wave with wavenumber $k_0 = 2\pi f/c_0$ where c_0 is an assumed sound speed. Technically, $H_0^{(1)}$ is a Hankel function of the first kind of zero order. The aim of PE models is to solve for $f(r, z)$, which represents the way in which the true field varies from that produced by the ideal outgoing cylindrical wave.

If the sound is assumed to be propagating predominantly in the range direction (the so-called paraxial approximation), then an efficient numerical algorithm can be employed. Given $f(r, z)$, a small range step dr is added to calculate $f(r + dr, z)$, a little bit farther from the source. This calculation can then be repeated as many times as desired to march the solution out in range. The sound field at one range is thus used to calculate the sound field at the next range and so on, without explicitly solving the depth-separated Helmholtz equation, making this a fundamentally different approach to the normal mode and wavenumber integration methods discussed previously.

Initially, the paraxial approximation was very restrictive and severely limited the utility of PE models for solving underwater acoustics problems. The more recent development of so-called high-angle PE models greatly relaxed this approximation. The way in which the solution marches out in range makes it straightforward to include range-dependent water depth, sound speed profiles, and seabed properties, and as a result, high-angle PE models have become the method of choice for solving range-dependent propagation problems.

Perhaps the most widely used PE model is *RAM* (Collins 1993), which allows the user a trade-off between the valid angular range and computational efficiency by specifying the number of terms to be used in a Padé approximation, which is central to the wide-angle algorithm. The more terms that are used in the Padé approximation, the wider is the valid angular range. Even though this allows the paraxial approximation to be greatly relaxed, it cannot be completely eliminated, and so PE models should always be used with care when acoustic energy propagating at steep angles is significant.

Another consideration when running *RAM* or similar PE models is that they use a finite computational grid in the depth direction, and energy will be artificially reflected by the sudden truncation at the bottom of the grid. This is usually dealt with by including an extra attenuation layer underneath the layer representing the physical seabed. The attenuation layer has the same density and sound speed as the seabed but an artificially high attenuation coefficient so that little energy reaches the bottom of the grid, and any energy that does reflect is further attenuated before reappearing in the water column. A sudden change in attenuation can also lead to reflections, so in critical situations, it is advisable to ramp the attenuation up smoothly from its seabed value to a high value, rather than having a step change.

There are several variants of *RAM* intended for different purposes (Table 6.1). The only one that can deal with elastic seabeds is *RAMS*, but it requires careful tuning of parameters to avoid instability, and in some cases involving layered seabeds, it is impossible to obtain a stable solution. More recent PE models have been developed that overcome these limitations (Collis et al. 2008) yet are research codes not readily

[7] *OASES* code https://oceanai.mit.edu/lamss/pmwiki/pmwiki.php?n=Site.Oases; accessed 1 October 2020.

Table 6.1 Summary of variants of the *RAM* parabolic-equation codes

Program	Seabed layering	Seabed type	Sea surface
RAM	Specified relative to the sea surface. Bathymetry cuts through the stack of layers.	Fluid only	Flat
RAMSurf	As for RAM.	Fluid only	Specified profile
RAMGeo	Specified relative to the seabed. Layering follows bathymetry.	Fluid only	Flat
RAMS	As for RAM.	Elastic	Flat

available. The majority of PE codes are intended for $N \times$ 2D modeling. However, research-level 3D PE codes have been developed (see Jensen et al. 2011, Sect. 6.8, for details).

6.4.5 Choosing the Most Appropriate Model

If the frequency is high enough that the acoustic wavelength is less than a small fraction of the smallest significant feature in the sound speed profile (e.g., mixed layer thickness, water depth), then use a ray tracing or beam model (e.g., *Bellhop*), otherwise use one of the low-frequency models. A rule of thumb for the 'small fraction' is 1/100. However, accurately modeling sound propagation in a weak duct may require the use of a low-frequency model up to a higher frequency than this rule would suggest. If in doubt, run some tests using both types of models to determine the frequency at which the two models start to agree.

When choosing a low-frequency model, if the range is short enough that the environment can be considered range-independent, then pick a wavenumber integration model (e.g., *OASES* or *SCOOTER*), otherwise use a PE model (e.g., *RAM*). The benefit of wavenumber integration for range-independent modeling is its greater accuracy at short range compared to either a normal-mode model (which only considers trapped energy) or a PE model (which has high-angle limitations). Wavenumber integration can also deal accurately with elastic seabed effects, which tend to be most important at short range. PE codes have largely replaced normal-mode codes for range-dependent modeling because of the greater practicality of the PE range-marching algorithm.

Range-dependent modeling with layered elastic seabeds remains a difficult computational task. One commonly resorts to work-around strategies, such as replacing the true seabed with an "equivalent" fluid seabed that has a similar reflection coefficient versus grazing angle dependence at low grazing angles. This allows a standard PE code to be used for the modeling but is only accurate at ranges large enough that there is no high-angle energy reaching the receiver.

6.4.6 Accessing Acoustic Propagation Models

Many of the models described in this chapter are freely available for download from the Ocean Acoustics Library[8] (OALIB). OALIB includes Michael D. Porter's *Acoustics Toolbox*, which incorporates a Gaussian beam tracing model (*Bellhop*), wavenumber integration code (*SCOOTER*), normal-mode model (*KRAKEN*), as well as several other useful programs including one for calculating seabed reflectivity as a function of grazing angle for arbitrarily complicated, layered seabeds (*BOUNCE*). These all use similar input and output file formats, have been regularly updated until at least 2020, and are well documented. A number of *MATLAB* (The MathWorks Inc., Natick, MA, USA) routines for dealing with the input and output are also provided. Also available on OALIB is the free version of the wavenumber integration code

[8] Ocean Acoustics Library https://oalib-acoustics.org/; accessed 17 June 2020.

OASES and a number of different PE codes, including the *RAM* family.

Unfortunately, downloading a particular code is often just the start of a journey that may include compiling it for the particular operating system you are using, deciphering the documentation to determine what input files are required and how they need to be formatted, and then working out how to read and plot the output data. There are usually a number of adjustable parameters that affect how the program operates, and it is necessary to have an understanding of the underlying numerical methods in order to set these appropriately. Inappropriate parameter selection will often lead to meaningless results, so whenever you start using a different propagation model, you should run a series of tests on simple problems (to which the answer is known) in order to make sure you are getting the correct results. The standard of documentation varies considerably between the different models that are available from OALIB and is minimal for some.

AcTUP[9] is a *MATLAB* GUI to earlier (2005) versions of the *Acoustics Toolbox* and several of the *RAM* family of PE codes. *AcTUP* comes packaged with the required Windows executables. This provides a convenient entry point for those new to acoustic propagation modeling as it allows different codes to be run on the same problem with minimal changes. However, careful parameter selection is still required in order to get meaningful results; put garbage in, get garbage out.

6.5 Practical Acoustic Modeling Examples

Having worked through the theory and concepts, this section finally puts all of the above into action and provides examples of some practical acoustic propagation modeling tasks of increasing complexity. These all involve the estimation of received levels due to a source with known sound emission characteristics, and are conceptually based on re-arranging the passive sonar equation (Eq. 6.1) to solve for the received level *RL*:

$$RL = SL - PL. \tag{6.16}$$

The tasks are:

1. Calculate *RL* as a function of range and depth in a given direction from a tonal (i.e., single-frequency) source.
2. Calculate *RL* as a function of range and depth in a given direction from a broadband source.
3. Calculate *RL* as a function of geographical position and depth for an omnidirectional source in a directional environment.
4. Calculate *RL* as a function of geographical position and depth for a directional source in a directional environment.

Indicative execution times are given for calculations that were carried out on a desktop computer with an Intel i7–7700 CPU, a clock speed of 3.6 GHz, and 64 GB of RAM. The processor had 4 physical cores but the models used here were single-threaded so only used one core. The computer was running a 64-bit Windows 10 operating system.

6.5.1 Received Level Versus Range and Depth from a Tonal Source

For this case, it is only necessary to specify the acoustic environment (i.e., bathymetry profile, sound speed profile, and seabed properties) along a single azimuth from the source. The propagation loss *PL* is only required at the source transmission frequency, and can be obtained using a single run of an appropriate propagation model. The received level *RL* can then be obtained using Eq. (6.16).

The example of a fin whale (*Balaenoptera physalus*) located about 40 km off the coast of southwestern Australia, at a depth of 50 m, while emitting a 20-Hz tone at a source level of 189 dB re 1 µPa m (Sirovic et al. 2007) is depicted in Fig. 6.16. The modeled direction of propagation

[9] *AcTUP* http://cmst.curtin.edu.au/products/underwater/download/; accessed 1 October 2020.

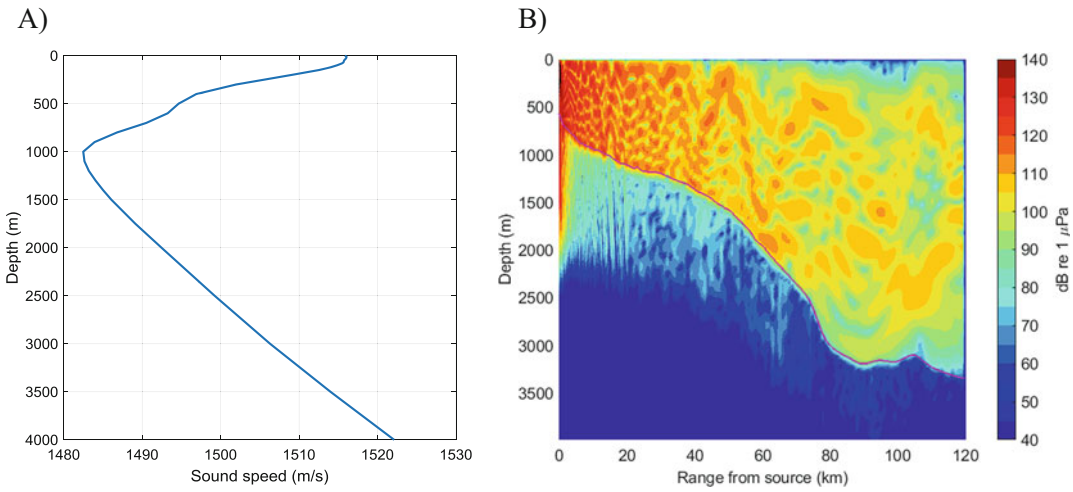

Fig. 6.16 (**a**) Sound speed profile used for the modeling examples. (**b**) Modeled received SPL as a function of range and depth for a fin whale at a depth of 50 m emitting a 20-Hz tone with a source level of 189 dB re 1 μPa m. The magenta line is the seafloor

was due west from the source, and the bathymetry profile (i.e., magenta line in Fig. 6.16b) was interpolated from the Geosciences Australia 0.15′ resolution bathymetry database.[10] The sound speed profile (Fig. 6.16a) was calculated from salinity and temperature data obtained from the *World Ocean Atlas* (Locarnini et al. 2018; Zweng et al. 2018). The seabed was modeled as a fine sand half-space with parameters from Jensen et al. (2011). Propagation loss modeling was carried out with *RAMGeo* in *AcTUP*, which is very efficient at such a low frequency, taking only a few seconds. A simple program was written in *MATLAB* to read the propagation loss file produced by *RAMGeo*, calculate the received levels using Eq. (6.16), and plot the results. Note that *AcTUP* can be used to plot propagation loss, but not received level.

The sound field has a complicated structure of peaks and nulls that is the result of constructive and destructive interference between sound that has traveled from the source to the receiver via different paths. This is typical of the sound fields produced by tonal sources. The overall reduction in received level with increasing range is quite slow, particularly beyond 70 km, due to the sound becoming constrained by refraction in the deep sound channel. This is typical of downslope propagation from a near-surface source situated over the continental slope into deep water.

6.5.2 Received Level Versus Range and Depth from a Broadband Source

Many sources of underwater sound are broadband, which means that they produce significant acoustic output over a wide range of frequencies. Ships, pile driving, and the airgun arrays used for seismic surveying all produce broadband noise, and modeling the resulting sound fields is of importance when assessing the potential impacts of these sources on marine animals.

A common way to carry out broadband modeling for continuous sound such as ship noise is:

[10] Whiteway, T., Australian Bathymetry and Topography Grid, June 2009, https://ecat.ga.gov.au/geonetwork/srv/eng/catalog.search#/metadata/67703; accessed 6 November 2020.

1. Break the required frequency span into a series of frequency bands (e.g., 1/3 octave bands are commonly used; see Chap. 4).
2. Use a propagation model to estimate a typical propagation loss for each band. This can either be done by running the propagation loss model at the center frequency of each band or by running it at a number of frequencies within the band and then averaging the results. The latter is preferred as it smooths out the interference field to some extent, but if the source emits a wide range of frequencies that span many bands, then the two methods will yield very similar results for the total field.
3. Integrate the source power spectral density over each band and convert to a source level.
4. Use Eq. (6.16) to obtain the received level in each band.
5. Sum the corresponding mean-square pressures across the bands to obtain an overall mean-square pressure that can then be converted to an overall received sound pressure level (SPL, see Chap. 4).

The use of mean-square pressure as a metric is problematic for impulsive sources such as airguns or pile driving, because the results become very sensitive to the duration of the signal, which is often hard to determine. Source and received levels for impulsive sources are therefore usually characterized in terms of sound exposure, and its logarithmic measure, the sound exposure level (SEL, see Chap. 4).

Computing the received levels for impulsive sources follows the same steps as for broadband, continuous sources, except that in step 3, the source spectrum needs to be specified as an energy density spectrum instead of a power density spectrum, and in step 5, it is sound exposures that are summed across the bands to obtain the overall sound exposure, which is then converted to a sound exposure level.

As an example, the modeled received sound exposure levels due to a single 3.3-l (200-cui) airgun are plotted as a function of range and depth in Fig. 6.17. The airgun (i.e., a cylindrical tube filled with compressed air, which is suddenly released into the water) is located at the geographical location that was used for the fin whale example, but at a depth of 6 m, which is typical of seismic survey source depths. The scenario is otherwise the same as previously described. The airgun's source waveform was modeled using the *Cagam* airgun array model (Duncan and Gavrilov 2019). The airgun array model also calculated the signal's energy density spectrum, which was then used in step 3 of the broadband modeling procedure outlined above. Once again, *AcTUP* was used to run *RAMGeo* to carry out the propagation modeling, but this time at 1/3 octave band center frequencies from 7.9 Hz to 1 kHz, which took about 5 minutes. A separate *MATLAB* program was written to carry out the post-processing steps and to plot the results.

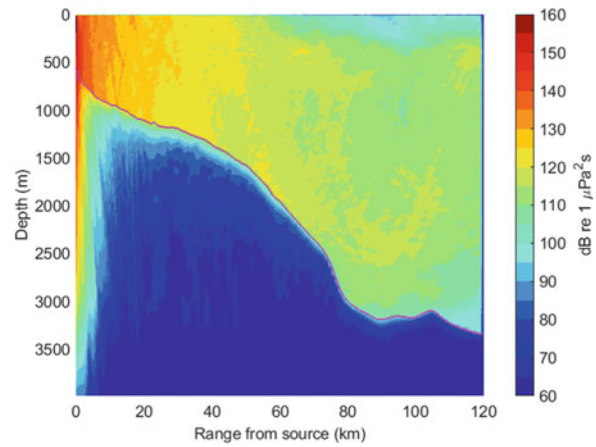

Fig. 6.17 Received SEL from a 3.3-l (200-cui) airgun at a depth of 6 m as a function of range and depth. The magenta line is the seafloor

Comparing Fig. 6.17 with Fig. 6.16, it can be seen that the broad range of frequencies emitted by the airgun has the effect of smoothing out the fluctuations in the sound field caused by interfering paths. The color scales on these two figures are not directly comparable because Fig. 6.16 gives SPL in dB re 1 μPa whereas Fig. 6.17 presents SEL in dB re 1 $\mu Pa^2 s$. The two are related through:

$$SEL = SPL + 10 \log_{10} T \tag{6.17}$$

where T is the duration of the received signal in seconds, conventionally defined as the duration of the time interval containing 90% of the signal's energy (90% energy signal duration; see Chap. 4).

6.5.3 Received Level as a Function of Geographical Position and Depth

The geographical distribution of received sound levels can be modeled by repeating the tonal source modeling procedure (Sect. 6.5.1) or broadband source modeling procedure (Sect. 6.5.2) using bathymetry profiles appropriate for different directions from the source. For long-range modeling, it may also be necessary to make the sound speed profile a function of range and direction. This is called $N \times$ 2D modeling and is adequate in most circumstances, but is less accurate than running a fully 3D propagation model in situations involving sound propagating across steeply sloping seabeds, or in some special situations in which horizontal sound speed gradients become significant.

The result is a 3D grid of the received level as a function of range, depth, and azimuth (i.e., direction in the horizontal plane). To create a 2D map of the sound field, it is necessary to extract some measure of the sound field in the vertical dimension and then interpolate that in the horizontal plane, with the appropriate measure depending on the purpose of the modeling. For example, in environmental impact assessments, it is common to use the maximum level at any depth in the water column, or the maximum level in a depth range corresponding to the diving range of an animal of interest.

Here we illustrate $N \times$ 2D modeling using the previous two examples, but this time carrying out the propagation modeling with bathymetry appropriate for each of the 37 tracks shown in Fig. 6.18. These were set at 10° increments in azimuth, with some adjustment and an extra track inserted in the inshore direction to improve the definition of the received field in the vicinity of the two capes. *MATLAB* programs were written to automate the various steps of the process.

Results are plotted in Fig. 6.19 for the fin whale and the airgun. In both cases, the plots are of the maximum received level over depth, but once again, they are not directly comparable because SPL was plotted for the fin whale, whereas SEL was plotted for the airgun.

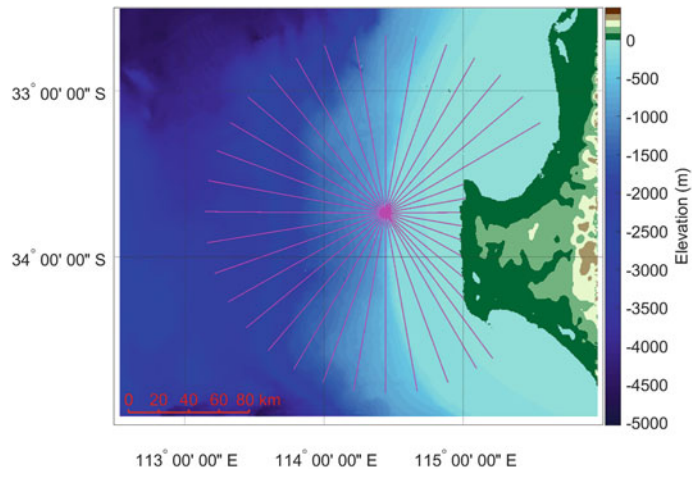

Fig. 6.18 Map showing the bathymetry off the southwest coast of Australia. The lines radiating from the chosen source location show the tracks along which propagation was modeled

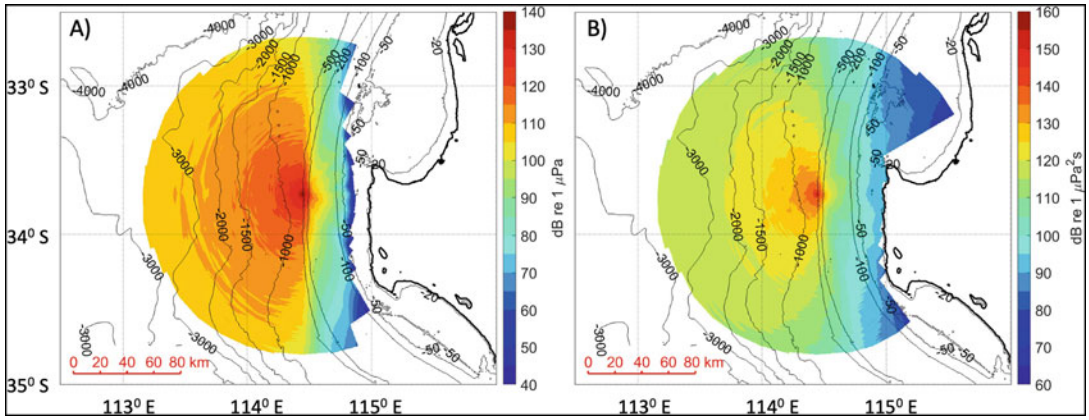

Fig. 6.19 (**a**) Map of maximum SPL over depth as a function of geographical position due to a fin whale calling at a depth of 50 m off the southwest coast of Australia. (**b**) Map of maximum SEL over depth due to a single firing of an airgun of volume 3.3 l (200 cui) at a depth of 6 m

6.5.4 Received Level as a Function of Geographical Position and Depth for a Directional Source

Another level of complexity occurs when the source emits sound differently in different directions. We illustrate this for an airgun array typical of those used for offshore seismic surveys. In this case, the array consists of 30 individual airguns of different sizes arranged in a 21-m wide by 15-m long rectangular array, with all airguns at the same depth of 6 m. The total volume of the compressed air released when the airguns fire is 55.7 l (3400 cui), and the tow direction is towards the North. The *Cagam* airgun array model was used to calculate a representative source spectrum corresponding to the direction of each of the propagation tracks shown in Fig. 6.18. Apart from using a different source spectrum for each direction, the procedure for calculating the received levels was identical to that described in the previous section for the single airgun.

The maximum received SEL at any depth is plotted in Fig. 6.20a, which uses the same color scale as Fig. 6.19b. The array produced higher levels overall, and the sound field was more directional, with distinct maxima east, west, and to a lesser extent, north and south from the source. Figure 6.20b combines range-depth plots for the 90° and 270° azimuths in a single plot, which illustrates the contrasting sound attenuation rates in the upslope and downslope directions.

6.5.5 Modeling Limitations and Practicalities

Provided the chosen propagation modeling approach is appropriate for the task, the largest uncertainties in the results are likely due to a lack of information on the environment, which includes the bathymetry, seabed composition, and water column sound speed profile. Bathymetry and water column sound speed profiles are often straightforward to measure or can be obtained from databases, but knowledge of the acoustic properties of the seabed is often poor (i.e., unavailable, patchy, and uncertain) and the parameters that contribute to the geoacoustics (e.g., sediment composition, density, and thickness) vary over space and not coherently (Erbe et al. 2021). Moreover, seabed properties tens or even hundreds of meters below the seafloor may be important when modeling low-frequency propagation (Etter 2018). As a result, it is often prudent to carry out modeling with several

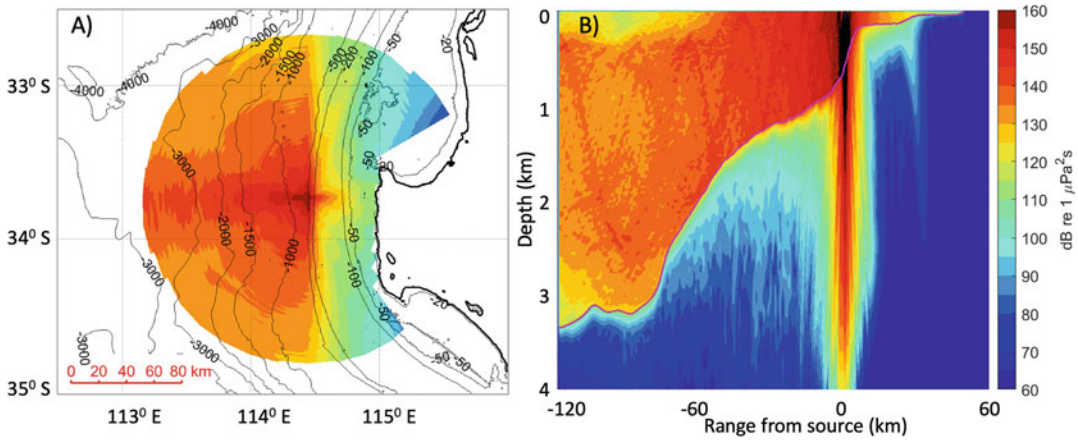

Fig. 6.20 (**a**) Map of maximum SEL over depth as a function of geographical position due to a single firing of a typical airgun array off the southwest coast of Australia. The total volume of the airguns in the array was 55.7 l (3400 cui), and the array was at a depth of 6 m. The tow direction of the array was northwards. (**b**) Received SEL from the same airgun array as a function of range and depth. The source was at 0-km range, negative ranges correspond to the 270° azimuth (i.e., west of the source) and positive ranges correspond to the 90° azimuth (i.e., east of the source). The magenta line is the seafloor. Colorbar applies to both panels

different sets of seabed properties in order to obtain an estimate of the uncertainty in the results.

The use of $N \times$ 2D rather than fully 3D modeling in the above examples may introduce some inaccuracies for cross-slope propagation paths, which in this case are to the north and south of the source. The effect of the sloping bathymetry would be to deflect the sound towards the downslope direction, slightly increasing levels downslope and decreasing them upslope.

The modeling methods described above treat the source as an ideal point source, which is a good approximation provided the receiver is much farther away from the source than the dimensions of the source. Modeling received levels close to a large source such as an airgun array requires a different and more computationally intensive approach in which the individual airguns in the array are treated as separate sources, and their signals are combined, taking account of their relative phases at the receiver locations. The same approach accounts for the full 3D directivity of the source, rather than just the horizontal directivity, as was the case for the example in Sect. 6.5.4. Combining this approach with a process called Fourier synthesis (Jensen et al. 2011) allows the received waveforms to be simulated, which allows other signal measures such as peak sound pressure levels (SPL_{pk}) to be calculated. Calculating SPL_{pk} by this means works well at short ranges but tends to overestimate levels at longer ranges because the propagation models do not properly account for seabed and sea surface scattering effects that broaden the peaks and reduce their amplitudes.

Simple propagation modeling tasks such as those described in Sects. 6.5.1 and 6.5.2 can be carried out using free propagation modeling tools such as the *Acoustics Toolbox* and *AcTUP*, with the addition of some relatively straightforward post-processing coded in any convenient programming language. However, when $N \times$ 2D modeling in multiple directions is required, it becomes desirable to automate the process of interpolating bathymetry profiles from databases, generating sound speed profile files, initiating multiple runs of the propagation model, calculating received levels, interpolating and plotting results, etc. Most organizations that routinely carry out this type of modeling have written their own proprietary software for these tasks. To the authors' knowledge, there is no freely available software package with all of these capabilities, although there is at least one commercially available package.

6.6 Summary

Sound propagation under water is a complex process. Sound does not propagate along straight-line transmission paths. Rather, it reflects, refracts, and diffracts. It scatters off rough surfaces (such as the sea surface and the seafloor) and off reflectors within the water column (e.g., gas bubbles, fish swim bladders, and suspended particles). It is transmitted into the seafloor and partially lost from the water. It is converted into heat by exciting molecular vibrations. There are common misconceptions about sound propagation in water, such as "low-frequency sound does not propagate in shallow water," "over hard seafloors, all sound is reflected, leading to cylindrical spreading," and "over soft seafloors, sound propagates spherically." This chapter aimed to remove common misconceptions and empower the reader to comprehend sound propagation phenomena in a range of environments and appreciate the limitations of widely used sound propagation models. The chapter began by deriving the sonar equation for a number of scenarios including animal acoustic communication, communication masking by noise, and acoustic surveying of animals. It introduced the concept of the layered ocean, presenting temperature, salinity, and resulting sound speed profiles. These were needed to develop the most common concepts of sound propagation under water: ray tracing and normal modes. The chapter computed Snell's law, reflection and transmission coefficients, and Lloyd's mirror. It provided an overview of publicly available sound propagation software (including wavenumber integration and parabolic equation models). It concluded with a few practical examples of modeling propagation loss for whale song and a seismic airgun array.

6.7 Additional Resources

- Dan Russell's Acoustics and Vibration Animations: https://www.acs.psu.edu/drussell/demos.html
- The Discovery of Sound in the Sea (DOSITS; https://dosits.org/) website has over 400 pages of content in three major sections including the science of underwater sound and how people and marine animals use underwater sound to conduct activities for which light is used in air. The website has been the foundational resource of the DOSITS Project, providing information at a beginner and advanced level, based on peer-reviewed science (Vigness-Raposa et al. 2016, 2019). The web structure has been transformed into structured tutorials that provide a streamlined, progressive development of knowledge. The tutorial layout allows a user to proceed from one topic to the next in sequence or jump to a specific topic of interest. The three tutorials focus on the science of underwater sound, the potential effects of underwater sound on marine animals, and the ecological risk assessment process for determining possible effects from a specific sound source. Additional resources have been developed to provide the underwater acoustics content in different formats, including instructional videos and webinars. Finally, there are print publications (an educational booklet and a trifold brochure) available in hard copy or PDF format and two eBooks available for free on the iBooks Store, including Book I: Importance of Sound in the Sea and Book II: Science of Underwater Sound.

References

Ainslie MA (2005) Effect of wind-generated bubbles on fixed range acoustic attenuation in shallow water at 1–4 kHz. J Acoust Soc Am 118(6):3513–3523. https://doi.org/10.1121/1.2114527

Ainslie MA, McColm JG (1998) A simplified formula for viscous and chemical absorption in sea water. J Acoust Soc Am 103(3):1671–1672. https://doi.org/10.1121/1.421258

American National Standards Institute (2015) Bioacoustical Terminology (ANSI S3.20-2015, R 2020). Acoustical Society of America, New York

Au WWL, Moore PWB (1984) Receiving beam patterns and directivity indices of the Atlantic bottlenose dolphin *Tursiops truncatus*. J Acoust Soc Am 75(1):255–262. https://doi.org/10.1121/1.390403

Benoit-Bird KJ, Waluk CM (2020) Exploring the promise of broadband fisheries echosounders for species discrimination with quantitative assessment of data processing effects. J Acoust Soc Am 147(1):411–427. https://doi.org/10.1121/10.0000594

Benoit-Bird KJ, Moline MA, Southall BL (2017) Prey in oceanic sound scattering layers organize to get a little help from their friends. Limnol Oceanogr 62(6): 2788–2798. https://doi.org/10.1002/lno.10606

Collins MD (1993) An energy-conserving parabolic equation for elastic media. J Acoust Soc Am 94(2):975–982

Collis JM, Siegmann WL, Jensen FB, Zampolli M, Küsel ET, Collins MD (2008) Parabolic equation solution of seismo-acoustics problems involving variations in bathymetry and sediment thickness. J Acoust Soc Am 123(1):51–55. https://doi.org/10.1121/1.2799932

Duncan AJ, Gavrilov AN (2019) The CMST Airgun Array model—a simple approach to modeling the underwater sound output from seismic Airgun arrays. IEEE J Ocean Eng 44(3):589–597. https://doi.org/10.1109/JOE.2019.2899134

Erbe C (2000) Detection of whale calls in noise: performance comparison between a beluga whale, human listeners and a neural network. J Acoust Soc Am 108(1):297–303. https://doi.org/10.1121/1.429465

Erbe C (2002) Underwater noise of whale-watching boats and its effects on killer whales (*Orcinus orca*). Mar Mamm Sci 18(2):394–418. https://doi.org/10.1111/j.1748-7692.2002.tb01045.x

Erbe C (2008) Critical ratios of beluga whales (*Delphinapterus leucas*) and masked signal duration. J Acoust Soc Am 124(4):2216–2223. https://doi.org/10.1121/1.2970094

Erbe C (2015) The maskogram: a tool to illustrate zones of masking. Aquat Mamm 41(4):434–443. https://doi.org/10.1578/AM.41.4.2015.434

Erbe C, Farmer DM (1998) Masked hearing thresholds of a beluga whale (*Delphinapterus leucas*) in icebreaker noise. Deep Sea Res II 45(7):1373–1388. https://doi.org/10.1016/S0967-0645(98)00027-7

Erbe C, Liong S, Koessler MW, Duncan AJ, Gourlay T (2016a) Underwater sound of rigid-hulled inflatable boats. J Acoust Soc Am 139(6):EL223–EL227. https://doi.org/10.1121/1.4954411

Erbe C, Parsons M, Duncan AJ, Allen K (2016b) Underwater acoustic signatures of recreational swimmers, divers, surfers and kayakers. Acoust Aust 44(2): 333–341. https://doi.org/10.1007/s40857-016-0062-7

Erbe C, Reichmuth C, Cunningham KC, Lucke K, Dooling RJ (2016c) Communication masking in marine mammals: a review and research strategy. Mar Pollut Bull 103:15–38. https://doi.org/10.1016/j.marpolbul.2015.12.007

Erbe C, Dunlop R, Jenner KCS, Jenner M-NM, McCauley RD, Parnum I, Parsons M, Rogers T, Salgado-Kent C (2017a) Review of underwater and in-air sounds emitted by Australian and Antarctic marine mammals. Acoust Aust 45:179–241. https://doi.org/10.1007/s40857-017-0101-z

Erbe C, Parsons M, Duncan AJ, Osterrieder S, Allen K (2017b) Aerial and underwater sound of unmanned aerial vehicles (UAV, drones). J Unmanned Veh Syst 5(3):92–101. https://doi.org/10.1139/juvs-2016-0018

Erbe C, Williams R, Parsons M, Parsons SK, Hendrawan IG, Dewantama IMI (2018) Underwater noise from airplanes: an overlooked source of ocean noise. Mar Pollut Bull 137:656–661. https://doi.org/10.1016/j.marpolbul.2018.10.064

Erbe C, Peel D, Smith JN, Schoeman RP (2021) Marine acoustic zones of Australia. J Mar Sci Eng 9(3):340. https://doi.org/10.3390/jmse9030340

Etter PC (2018) Underwater acoustic modeling and simulation, 5th edn. CRC Press, Boca Raton, FL. https://doi.org/10.1201/9781315166346

Fletcher H (1940) Auditory patterns. Rev Mod Phys 12: 47–65

François RE, Garrison GR (1982a) Sound absorption based on ocean measurements: part I: pure water and magnesium sulphate contributions. J Acoust Soc Am 72(3):896–907

François RE, Garrison GR (1982b) Sound absorption based on ocean measurements: part II: boric acid contribution and equation for total absorption. J Acoust Soc Am 72(6):1879–1890

Godin OA (2008) Sound transmission through water–air interfaces: new insights into an old problem. Contemp Phys 49(2):105–123. https://doi.org/10.1080/00107510802090415

Goh JT, Schmidt H (1996) A hybrid coupled wavenumber integration approach to range-dependent seismoacoustic modeling. J Acoust Soc Am 100(3): 1409–1420. https://doi.org/10.1121/1.415988

Hall MV (1989) A comprehensive model of wind-generated bubbles in the ocean and predictions of the effects on sound propagation at frequencies up to 40 kHz. J Acoust Soc Am 86(3):1103–1117. https://doi.org/10.1121/1.398102

Hall MV (2004) Preliminary analysis of the applicability of adiabatic modes to inverting synthetic acoustic data in shallow water over a sloping sea floor. IEEE J Ocean Eng 29(1):51–58. https://doi.org/10.1109/JOE.2003.823315

Jensen FB, Kuperman WA, Porter MB, Schmidt H (2011) Computational Ocean acoustics, 2nd edn. Springer, New York

Kloser RJ, Macaulay GJ, Ryan TE, Lewis M (2013) Identification and target strength of orange roughy (Hoplostethus atlanticus) measured in situ. J Acoust Soc Am 134(1):97–108

Koessler MW (2016) Modelling of underwater acoustic propagation over elastic, range-dependent seabeds. Ph. D. Thesis, Curtin University, Perth, WA, Australia

Kuehne LM, Erbe C, Ashe E, Bogaard LT, Collins MS, Williams R (2020) Above and below: military aircraft noise in air and under water at Whidbey Island, Washington. J Mar Sci Eng 8(11):923. https://doi.org/10.3390/jmse8110923

Locarnini RA, Mishonov AV, Baranova OK, Boyer TP, Zweng MM, Garcia HE, Reagan JR, Seidov D, Weathers K, Paver CR, Smolyar I (2018) World Ocean atlas 2018, volume 1: temperature. National Oceanic and Atmospheric Administration

Mackenzie KV (1981) Nine-term equation for sound speed in the oceans. J Acoust Soc Am 70:807–812

Medwin H, Clay CS (1998) Chapter 2 - sound propagation. In: Medwin H, Clay CS (eds) Fundamentals of acoustical oceanography. Academic Press, San Diego, pp 17–69. https://doi.org/10.1016/B978-012487570-8/50004-0

Moore BCJ (2013) An introduction to the psychology of hearing. Brill, Leiden, The Netherlands

Parsons MJG, Parnum IM, Allen K, McCauley RD, Erbe C (2014) Detection of sharks with the Gemini imaging sonar. Acoust Australia 42(3):185–189

Parsons MJG, Duncan AJ, Parsons SK, Erbe C (2020) Reducing vessel noise: an example of a solar-electric passenger ferry. J Acoust Soc Am 147(5):3575–3583. https://doi.org/10.1121/10.0001264

Porter MB (1990) The time-marched fast-field program (FFP) for modeling acoustic pulse propagation. J Acoust Soc Am 87(5):2013–2023. https://doi.org/10.1121/1.399329

Porter MB, Bucker HP (1987) Gaussian beam tracing for computing ocean acoustic fields. J Acoust Soc Am 82(4):1349–1359. https://doi.org/10.1121/1.395269

Porter M, Reiss EL (1984) A numerical method for ocean-acoustic normal modes. J Acoust Soc Am 76(1):244–252. https://doi.org/10.1121/1.391101

Schmidt H, Glattetre J (1985) A fast field model for three-dimensional wave propagation in stratified environments based on the global matrix method. J Acoust Soc Am 78(6):2105–2114. https://doi.org/10.1121/1.392670

Sirovic A, Hildebrand JA, Wiggins SM (2007) Blue and fin whale call source levels and propagation range in the Southern Ocean. J Acoust Soc Am 122(2):1208–1215. https://doi.org/10.1121/1.2749452

Urick RJ (1983) Principles of underwater sound, 3rd edn. McGraw Hill, New York

Vigness-Raposa KJ, Scowcroft G, Morin H, Knowlton C, Miller JH, Ketten DR, Popper AN (2016) Discovery of sound in the sea: resources for decision makers. Proc Meet Acoust 27(1):010008. https://doi.org/10.1121/2.0000257

Vigness-Raposa KJ, Scowcroft G, Morin H, Knowlton C, Miller JH, Ketten DR, Popper AN (2019) Discovery of sound in the sea: communicating underwater acoustics research to decision makers. Proc Meet Acoust 37(1):025001. https://doi.org/10.1121/2.0001204

Westwood EK, Tindle CT, Chapman NR (1996) A normal mode model for acousto-elastic ocean environments. J Acoust Soc Am 100(6):3631–3645. https://doi.org/10.1121/1.417226

Zweng MM, Reagan JR, Seidov D, Boyer TP, Locarnini RA, Garcia HE, Mishonov AV, Baranova OK, Weathers K, Paver CR, Smolyar I (2018) World Ocean atlas 2018, volume 2: salinity. National Oceanic and Atmospheric Administration